Available online at www.sciencedirect.com

ScienceDirect

Russian Geology and Geophysics 57 (2016) 653–671

RUSSIAN GEOLOGY AND GEOPHYSICS

www.elsevier.com/locate/rgg

The 1501 Ma Kuonamka Large Igneous Province of northern Siberia: U–Pb geochronology, geochemistry, and links with coeval magmatism on other crustal blocks

R.E. Ernst [a,b,*], A.V. Okrugin [c], R.V. Veselovskiy [d,e], S.L. Kamo [f], M.A. Hamilton [f], V. Pavlov [d,g], U. Söderlund [h], K.R. Chamberlain [i], C. Rogers [a]

[a] *Department of Earth Sciences, Carleton University, Ottawa, ON, K1S 5B6, Canada*
[b] *Faculty of Geology and Geography, Tomsk State University, pr. Lenina 36, Tomsk, 634050, Russia*
[c] *Diamond & Precious Metal Geology Institute, Russian Academy of Sciences, pr. Lenina 39, Yakutsk, 677000, Russia*
[d] *Institute of Physics of the Earth, Russian Academy of Sciences, ul. Bol'shaya Gruzinskaya 10, build. 1, 123995, Moscow, Russia*
[e] *Geological Department, Lomonosov Moscow State University, ul. Leninskie Gory 1, 119991, Moscow, Russia*
[f] *Jack Satterly Geochronology Laboratory, University of Toronto, Toronto, ON, M5S 3B1, Canada*
[g] *Kazan Federal University, ul. Kremlevskaya 18, Kazan, 420000, Russia*
[h] *Department of Geology, Lund University, Lund, 223 62, Sweden*
[i] *Department of Geology and Geophysics, University of Wyoming, Laramie, Wyoming, 82071, USA*

Received 29 December 2015; accepted 29 January 2016

Abstract

A new large igneous province (LIP), the 1501 ± 3 Ma Kuonamka LIP, extends across 700 km of northern Siberia and is linked with coeval dikes and sills in the formerly attached São Francisco craton (SFC)–Congo craton to yield a short-duration event 2000 km across. The age of the Kuonamka LIP can be summarized as 1501 ± 3 Ma (95% confidence), based on 7 U–Pb ID-TIMS ages (6 new herein) from dolerite dikes and sills across the Anabar shield and within western Riphean cover rocks for a distance of 270 km. An additional sill yielded a SIMS (CAMECA) age of 1483 ± 17 Ma and sill in the Olenek uplift several hundred kilometers farther east, a previous SIMS (SHRIMP) age of ca. 1473 Ma was obtained on a sill; both SIMS ages are within the age uncertainty of the ID-TIMS ages. Geochemical data indicate a tholeiitic basalt composition with low MgO (4–7 wt%) within-plate character based on trace element classification diagrams and source between E-MORB and OIB with only minor contamination from crust or metasomatized lithospheric mantle. Two subgroups are distinguished: Group 1 has gently sloping LREE ($(La/Sm)_{PM} = 1.9$) and HREE ($(Gd/Yb)_{PM} = 1.8$) patterns, slightly negative Sr and moderate TiO_2 (2.2 wt%), and Group 2 has steeper LREE ($(La/Sm)_{PM} = 2.3$) and HREE ($(Gd/Yb)_{PM} = 2.3$), strong negative Sr anomaly, is higher in TiO_2 (2.7 wt%), and is transitional from tholeiitic to weakly alkaline in composition. The slight differences in REE slopes are consistent with Group 2 on average melting at deeper levels. Proposed reconstructions of the Kuonamka LIP with 1500 Ma magmatism of the SFC–Congo craton are supported by a geochemical comparison. Specifically, the chemistry of the Chapada Diamantina and Curaça dikes of the SFC can be linked to that of Groups 1 and 2, respectively, of the Kuonamka LIP and are consistent with a common mantle source between EMORB and OIB and subsequent differentiation history. However, the coeval Humpata sills and dikes of the Angola block of the Congo craton represent a different magma batch.

Keywords: magmatism; dikes; sills; igneous province; northern Siberia

Introduction

Large Igneous Provinces (LIPs) represent large volume (>0.1 Mkm^3; frequently above >1 Mkm^3), mainly mafic (ultramafic) magmatic events of intraplate affinity, that occur in both continental and oceanic settings, and are typically of short duration (<5 m.y.) or consist of multiple short pulses over a maximum of a few 10s of m.y. (Ernst, 2014 and references therein). They comprise volcanic packages (flood basalts), and a plumbing system of dikes, sills and layered intrusions, and can be associated with silicic magmatism, carbonatites and kimberlites. LIPs are linked with continental

* Corresponding author.
E-mail address: Richard.Ernst@ErnstGeosciences.com (R.E. Ernst)

1068-7971/$ - see front matter © 2016, V.S. Sobolev IGM, Siberian Branch of the RAS. Published by Elsevier B.V. All rights reserved.
http://dx.doi.org/10.1016/j.rgg.2016.01.015

breakup, global climate change including extinction events, and ore deposits of a variety of commodity types.

The Siberian craton is best known for the 252 Ma Siberian Trap Large Igneous Province (LIP), which covers several million km^2, was emplaced mostly within a million years and hosts the important Ni-Cu-PGE Noril'sk deposits (e.g., Burgess and Bowring, 2015; Ernst, 2014; Ivanov et al., 2013; Kamo et al., 2003; Naldrett, 2010; Reichow et al., 2009; Ryabov et al., 2014). Recently, Proterozoic LIPs of comparable scale to the Siberian Trap LIP have been discovered in Siberia through a campaign of U–Pb dating of dolerite dikes and sills by the LIPs Industry Consortium Project (www.supercontinent.org; Ernst et al., 2013a). For example a 1750 Ma giant radiating swarm extends over an area of >750,000 km^2 (e.g., Ernst et al., 2008; Gladkochub et al., 2010a,b). Furthermore, this and a number of other important southern Siberia LIPs can be linked with comparable age LIPs in northern Laurentia which indicates they were connected from 1.9–0.7 Ga (Ernst et al., 2015, 2016); thus increasing the size and advancing the importance of each of these LIPs.

Here we profile the 1500 Ma Kuonamka LIP of northern Siberia (Figs. 1 and 2; Ernst et al., 2014), which can also potentially be linked with dikes and sills in the formerly attached São Francisco–Congo craton (Ernst et al., 2013b) to delineate an event some 2000 km across (Fig. 3). We present new U–Pb ages, and geochemistry and consider the implications of a reconstruction with the São Francisco and Congo cratons.

Rock sample descriptions and locations

Sample locations are provided in Fig. 1 and Table 1, and some characteristics of the samples units are also listed in Table 1. Note that samples were provided by various co-authors, sampled at different times; details are provided below.

Dolerite dike samples of the EQ94 series: 01-01 (0.7 m wide), 02-05 (20 m wide), 03-05 (30 m wide), 04-05 (50 m wide), 13-01 (30-40 m wide) and 14-02 (35 m wide) were collected by R. Ernst and A. Okrugin during a 1994 sampling expedition along the Bolyshaya Kuonamka river in northern Siberia. Paleomagnetic results on these sites as well as a U–Pb baddeleyite age of 1503 ± 5 from site EQ94-04-05 were reported in Ernst et al. (2000). Previously reported K-Ar ages for some of these dikes include a date of 1242 ± 20 Ma at site EQ94-02, 1487 ± 10 Ma at site EQ94-03, 1391 ± 42 Ma at site EQ94-04, 1200 ± 8 Ma at site EQ94-13, 1537 ± 34 at site EQ94-14, and ages of 2728–2679 Ma reported by U–Pb ages on xenocrystic zircons at site EQ94-02 (Table 1 in Ernst et al., 2000).

In Ernst et al. (2000; and based on Okrugin et al., 1990) the EQ94 sites 01, 02, 03, 04 and 14 were linked, based on trend, composition, paleomagnetism, petrography and K–Ar ages, into the Kuonamka swarm and site 13 to the Juken swarm.

On the basis of geochemical evidence provided herein, the dolerite dike at site 13 instead appears correlative with the Kuonamka swarm.

Dolerite sill samples cutting Riphean cover rocks to the west of the Anabar shield include #11 (30 m thick), #14 (30 m thick), #24 (300 m thick), #81-108 (30 m thick), #139-153 (30 m thick), #181-200 (30 m thick), #215-225 (30 m thick), and #3 (100 m thick). In contrast, sample #259-273 (30 m thick) was collected from a dike. All samples in this series were collected by R. Veselovskiy.

Sample VP-2008 was collected by V. Pavlov from a dolerite sill (~15 m thick), exposed on the right bank of the Kotuykan River and the host rock is Riphean sandstones.

Sample F1 (Fomich River sill) for this study was collected by R. Veselovskiy and A. Shatsillo along the Fomich River in the Riphean cover of the 'northern slopes' of the Anabar uplift. Sample F1 is from a dolerite sill with a visible thickness of greater than 30 meters exposed on both banks of the Fomich River, about 10 km downstream from the mouth of the Burustakh brook. Four sills from the Fomich River valley studied previously yielded K-Ar ages of 912 Ma (for two sills), 1100 Ma and 1540 Ma (Kuteynikov et al., 1967). A Sm–Nd age of 1513 ± 51 Ma was also reported (Veselovskiy et al., 2006) on the same location as site F-1, dated in this report.

Samples AB81, AB85 and AB87 were collected by A. Okrugin along the Kotuykan River in the Riphean cover west of the Anabar shield. AB-81 and AB-87 are from 30 and 25 m thick dolerite sills, respectively, and AB-85 is from an ESE (110^o)-trending 50 m-wide dolerite dike. Previously reported K–Ar ages determined on these bodies include 1139 ± 31 Ma (AB-81), 1079 ± 45 Ma (AB-85), and 1314 ± 14 Ma (AB-87) (Okrugin et al., 1990).

Sample #22 was collected on the shore of the Kotuy river. The sill is about 300 m thick and was sampled from about 20 m from the margin. The host rocks are dolostones of the Usmastakh Formation (Pr2) or Staraya Rechka Formation (Vendian). This sill was sampled because it yields a very good paleomagnetic record (Veselovskiy and Pavlov, 2009). Previously, these rocks were considered as Vendian (or Permian-Triassic) in age, but paleomagnetic results indicate that they have about the same paleomagnetic direction as the other dolerites of age about 1500 Ma, a prediction that is confirmed by the U–Pb dating herein.

Petrography

All the collected samples have mineralogy of a dolerite with clinopyroxene and plagioclase as the main minerals and with minor Fe-Ti oxides and occasional apatite in a texture ranging from intersertal, to subophitic, to ophitic with increasing grain size. Minor alteration has partially sausseritized the plagioclase and uralitized the pyroxene. The two geochemical groups distinguished below on the base of trace element chemistry have the same mineralogy.

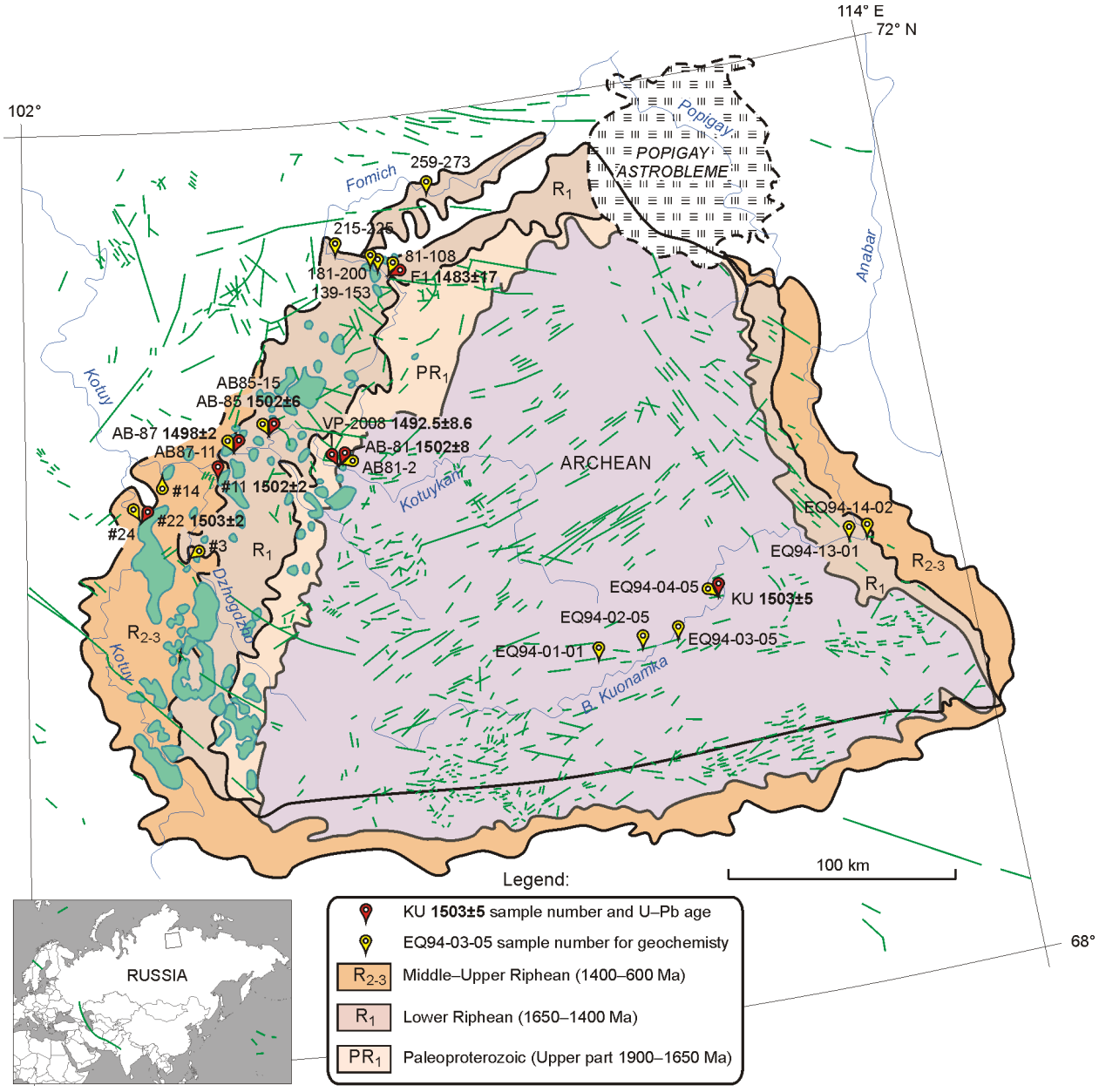

Fig. 1. Sample sites of Kuonamka LIP in the Anabar shield (Archean) and its Riphean (Mesoproterozoic to Neoproterozoic) cover sediments. The dikes (in green) represent a range of ages from Proterozoic to Paleozoic (e.g., Ernst et al., 2000; Okrugin et al., 1990), although the E–W dikes at the labelled sites along the Bolshaya Kuonamka river are known to represent Kuonamka dikes (Ernst et al., 2000). The sills (green polygons) in the Riphean cover rocks on the west side of the Anabar shield are thought to mainly belong to the Kuonamka LIP (based on the present study). Precambrian divisions are after ISC (2006) with the boundary between middle and lower Riphean after Puchkov et al. (2013).

Methodology

U–Pb ID-TIMS analytical procedures

Seven samples (Table 1) were dated by the U–Pb ID-TIMS (isotope dilution-thermal ionisation mass spectrometry) method. Baddeleyite was separated at Lund University and the University of Toronto geochronology laboratories using procedures similar to those described by Söderlund and Johansson (2002; see also Nilsson et al., 2013).

Recovered grains were analysed at the Jack Satterly Geochronology Laboratory at the University of Toronto for ID-TIMS dating. Final selection of unaltered baddeleyite grains for analysis was followed by cleaning in 7N HNO_3, and loading into Teflon capsules for dissolution with ~0.1 mL of hydrofluoric acid, ~0.02 mL of 7N HNO_3 and a mixed ^{205}Pb–^{235}U isotopic tracer solution for 3–4 days in an oven at ~195 °C, following the general procedures reported by Krogh (1973). Samples were then dried to a precipitate and redissolved in ~0.15 ml of 3N HCl overnight. U and Pb were isolated from the baddeleyite using 50 μL anion exchange columns using HCl, deposited onto outgassed rhenium filaments with silica gel (Gerstenberger and Haase, 1997), and

Table 1. Summary of Kuonamka LIP samples in this study

Sample	Latitude	Longitude	Form	Geochemical group	U–Pb age, Ma (by ID-TIMS except for F1)	Width of dike or sill, m	Trend (if dike)	Host rock
Group 1								
EQ94-01-01	69.54482	109.13160	Dike	1		0.7	E	Archean hypersthene and 2-pyroxene plagioclase gneiss
EQ94-02-05	69.59717	109.91635	Dike	1		40	E	Archean 2-pyroxene gneiss and pyroxene-plagioclase schist gneiss and schist
EQ94-04-05	69.76283	110.84697	Dike	1	1503 ± 5	50	E	Archean 2-pyroxene plagioclase gneiss and pyroxene plagioclase schist
AB85-15	70.67778	105.38333	Sill?	1	1502 ± 6	50		Riphean argillite, siltstone, conglomerate, sandstone, Ust'-Ilya and Labazt Fm.
AB87-11	70.60694	104.85833	Sill	1	1498 ± 2	25		Riphean dolomite, limestone, Kotuykan Fm.—Riphean sandstone, Ust'-Ilya Fm.
AB81-2	70.51806	106.12500	Sill	1	1502 ± 8	30		Paleoproterozoic sandstone, conglomerate, Ilya Fm.
139-153	71.36361	106.80556	Sill	1		30		Riphean dolomite, limestone, siltstone, sandstone, Ust'-Ilya Fm.
81-108 (= site F1)	71.34222	106.92444	Sill	1	1483 ± 17 (site F1; INSIMS method)	30		Riphean dolomite, limestone, siltstone, sandstone, Ust'-Ilya Fm.
14	70.51942	103.85536	Sill	1		30		Riphean dolomite, sandstone, Usmastakh Fm.
24	70.33783	103.53692	Sill	1	1503 ± 2 (at site 22)	300		Riphean dolomite, sandstone, Usmastakh Fm.
Group 2								
EQ94-13-01	69.90610	112.59757	Dike	2		30–40	ESE	Riphean dolomite, limestone, and argillite, Kotuykan Fm.
EQ94-14-02	69.89660	112.80077	Dike	2		35	E	Riphean dolomite, limestone, and argillite, Kotuykan Fm.
EQ94-03-05	69.61638	110.30357	Dike	2		30	E	Archean 2-pyroxene plagioclase gneiss and pyroxene plagioclase schist
259-273	71.64039	107.77389	Dike	2		30	NE	Riphean dolomite, limestone, and argillite, Kotuykan Fm.
215-225	71.40917	106.39056	Sill	2		30		Riphean dolomite, limestone, and argillite, Kotuykan Fm.
Group 2 (transitional to Group 1)								
11	70.49644	104.53350	Sill	2 (transitional between 1 and 2)	1501.6 ± 1.9	30		Riphean dolomite, limestone, and argillite, Kotuykan Fm.
No chemistry available								
VP-2008	70.51548	106.08947	Sill		1493 ± 9	15		Paleoproterozoic sandstone, conglomerate, Ilya Fm.
181-200	71.37167	106.72806	Sill			30		Riphean dolomite, limestone and argillite, Kotuykan Fm.
3	70.19294	104.11944	Sill			100		Riphean dolomite, limestone, and argillite, Kotuykan Fm.

Pb was analyzed with a VG354 mass spectrometer using a Daly detector in pulse counting mode. Estimates of fraction weights were made using measurements from digital imaging and the density of baddeleyite. System deadtime corrections during this period were 20 ns for Pb and 18 ns for U. Corrections for Daly mass bias were 0.07%/AMU (atomic mass unit), and thermal mass discrimination was taken to be 0.10%/AMU. Uranium–lead blanks in the laboratory normally average about 0.5 pg for Pb and 0.1 pg for U. Plotting and data regressions were carried out using the algorithms and software (Isoplot 3.0) developed by Ludwig (2003). All errors described here and in the plots (including error ellipses and calculated ages) are provided at the two-sigma level of uncertainty. Further details regarding analytical protocols are provided in Hamilton and Buchan (2010).

U–Pb IN-SIMS analytical procedures

Sample F1 was dated using the IN-SIMS (in situ, secondary ionization mass spectrometry) method. The first step in this method was locating zirconium-bearing phases in polished thin sections by wavelength dispersive spectroscopy (WDS, Uni-

versity of Wyoming). Each map required up to 10 hours of automated instrument time per section to locate the ~10 to 30 micron diameter target minerals. Manual energy dispersive spectroscopy (EDS) was used to identify the zirconium-bearing mineral phases. A series of back-scattered electron (BSE) and reflected light images at various magnifications were prepared to facilitate relocating the targets for isotopic analyses. 10 mm square, target-rich portions of the thin sections were mounted in 1 inch-diameter, epoxy disks along with prepolished standard grains for U and Pb isotopic analysis by secondary ion mass spectrometry (SIMS). SIMS analysis followed the methods described in Schmitt et al. (2010) and Chamberlain et al. (2010) using the CAMECA 1270*ims* at UCLA. Data were limited to the first 10 cycles following presputtering to minimize down-pit fractionation effects that have been occasionally observed, and the field aperture was matched to grain dimensions to screen out ions from host phases, especially common Pb. Sampling regions were generally limited to 3–4 microns of the 20-micron primary pit.

Major and trace element geochemistry

The dike and sill samples selected for major and trace element geochemical analysis were fresh and unmetamorphosed, and were processed into a fine rock powder at Carleton University prior to geochemical analysis. In the laboratory, samples were cut into multiple 1 cm thick slabs and any remaining weathering surface removed. A single representative slab was selected and flat surfaces were polished with 120-grit carborundum powder to remove any metal contamination introduced during the cutting process. Some of the slab material was repeatedly crushed and sieved until all crushed material was less than 2 mm before being milled to less than 200 mesh in an agate ring mill. The mill was precontaminated with an aliquot of each sample prior to the crushing and milling stages to produce the sample aliquot for analysis. Tools and working surfaces of the crusher and mill were cleaned with ethyl alcohol between each sample. These steps were used to reduce risk of cross-contamination of trace elements and isotopes between samples.

Approximately 20 g of <200 mesh sample were sent to ALS Laboratories (http://www.alsglobal.com/) for major, minor and trace element analysis. At ALS, samples were sintered with a lithium metaborate flux, before being analyzed for 55 major oxide and minor to trace elements via ICP-AES (inductively coupled plasma atomic emission spectrophotometry) and ICP-MS (inductively coupled plasma mass spectrometry). The sample analyses (Table A1) were normalized to 100% dry weight for plotting.

U–Pb geochronology

ID-TIMS method

New U–Pb ID-TIMS data are reported here for 7 samples (Table 2; Fig 2*A*–*E*).

EQ94-04-05: The initial preliminary age for this E–W trending dike collected along the Bolshaya Kuonamka River, at 1503 ± 5 Ma, was reported in Ernst et al. (2000). This determination was based on a model $^{207}Pb/^{206}Pb$ age from the analysis of a single, large multigrain baddeleyite fraction. In this study, we analyzed two additional smaller fractions comprising 7–8 crystals (mostly tiny blades and blade fragments) (Table 2; Fig. 2*A*). Both new analyses (Bd-2, Bd-3) are slightly more discordant than the original fraction (Bd-1), but all three yield similar model $^{207}Pb/^{206}Pb$ ages, between 1501.2–1503.0 Ma. Total common Pb is high in all measured fractions and appears to be intrinsic to the baddeleyite crystals themselves, possibly due to the presence of mineral inclusions. Proportionally higher ratios of common Pb in the new, smaller fractions results in relatively imprecise calculated Pb/U and Pb/Pb ratios, but a weighted average $^{207}Pb/^{206}Pb$ age of 1503.0 ± 4.6 Ma is confirmed for the primary age of this dike.

Site # 11: This 30 m-thick gabbro sill, collected along the Dzhogdzho River, intrudes the Usmastakh Formation in Riphean cover sediments of the western Anabar shield. The sample yielded a modest quantity of baddeleyite crystals, from which 4 fractions were selected for analysis, with each fraction comprising between 6–10 crystals. Analyzed fractions have Th/U ratios between 0.10–0.14 and range from 1.0–1.4% discordant. Model $^{207}Pb/^{206}Pb$ ages range from 1499.2–1503.8 Ma (Table 2). The data cluster slightly, but lie on a chord suggesting only modern Pb loss; together, the four data points provide a weighted average $^{207}Pb/^{206}Pb$ age of 1501.6 ± 1.9 Ma (MSWD = 0.79; Fig. 2*B*), interpreted to represent the age of emplacement and crystallization of the sill.

Site # 22: This gabbro sample, collected from a thick sill along the Kotuy River, contained a sparse amount of baddeleyite. Three baddeleyite fractions were analyzed, each comprising only 2–3 small, pale- to medium-brown blades and blade fragments, but each yielded concordant or near-concordant data, with $^{207}Pb/^{206}Pb$ ages ranging tightly between 1502.5–1503.2 Ma. A weighted average $^{207}Pb/^{206}Pb$ age of 1503.0 ± 2.0 Ma (MSWD = 0.4) is interpreted as the best estimate for the time of intrusion of this sill (Fig. 2*C* and Table 2).

VP-2008: This sample, from a 15 m-thick dolerite sill intruding Riphean sandstones along the Kotuykan River, yielded a modest amount of short or small medium brown baddeleyite blades or blade fragments, and rarer elongate crystals. Several fractions were selected for U–Pb TIMS analysis, each comprising between 2–11 grains. With the exception of a single normally discordant fraction (Bd-5) and a reversely-discordant fraction (Bd-4), most analyses fall within 0–3% of Concordia and, with the exception of imprecise analysis Bd-2, five points regress through the origin to yield an upper intercept age of 1492.7 ± 5.8 Ma (MSWD = 0.1; Table 2, Fig. 2*D*). The most concordant analyses have Th/U ratios consistent with good quality baddeleyite (~0.04–0.07), whereas those showing greater normal-discordance appear to correlate with higher ratios (up to 0.37) that likely reflect the presence of minor zircon overgrowths carrying alteration and associated Pb loss (e.g., Bd-1, Bd-5). An age

Table 2. U–Rb baddeleyite data for Kuonamka suite dolerite dikes and sills, northern Siberian craton

Fraction	Description	U, ppm	Pb^T, pg	Pb_c, pg	Th/U	$^{206}Pb/^{204}Pb$	$^{206}Pb/^{238}U$	±2σ	$^{207}Pb/^{235}U$	±2σ	$^{207}Pb/^{206}Pb$	±2σ	Ages, Ma						Disc., %
													$^{206}Pb/^{238}U$	±2σ	$^{207}Pb/^{235}U$	±2σ	$^{207}Pb/^{206}Pb$	±2σ	
Sample EQ94-04-05: E-W dolerite dike, Bolshaya Kuonamka River																			
Bd-1*	22 mbr el and short blades	224	67.8	2.8	0.10	1533	0.25812	0.00074	3.3363	0.0096	0.09375	0.00024	1480.2	3.8	1489.6	2.2	1503.0	4.8	1.7
Bd-2	8 mbr blades and frags	341	16.0	3.8	0.11	300	0.25728	0.00095	3.3224	0.0787	0.09366	0.00196	1475.9	4.9	1486.3	18.6	1501.2	39.9	19
Bd-3	7 mbr blades and frags	214	10.1	4 2	005	179	0.25635	0.00148	3.3120	0.1373	0.09370	0.00345	1471.1	7.6	1483.9	32.6	1502.1	70 4	23
Sample 11: gabbro sill, Dzhogdzho River area																			
Bd-1	6 pbr-mbr el blades and frags	335	27.1	0.7	0.10	2619	0.26002	0.00059	3.3624	0.0124	0.09379	0.00024	1489.9	3.0	1495.7	2.9	1503.8	4.8	1.0
Bd-2	7 pbr-mbr el blades and frags	381	39.3	0.5	0.14	5477	0.25856	0.00052	3.3398	0.0090	0.09368	0.00013	1482.5	2.7	1490.4	2.1	1501.7	2.7	14
Bd-3	10 pbr-mbr el blades and frags	309	30.4	0.6	0.10	3368	0.25851	0.00063	3.3347	0.0119	0.09356	0.00020	1482.2	3.2	1489.2	2.8	1499.2	4.1	13
Bd-4	10 pbr-mbr el blades and frags	400	45.0	2.0	0.10	1544	0 25926	0.00053	3.3509	0.0168	0.09374	0.00038	1486.1	2.7	1493.0	3.9	1502.9	7.6	13
Sample 22: gabbro sill, Kotuy River area																			
Bd-1	2 sm, pbr, in	243	62.6	0.7	0.11	880	0.26314	0.00118	3.4016	0.0140	0.09376	0.00018	1505.9	6.0	1504.8	3.2	1503.2	36	–0.2
Bd-2	3 short, pbr, elong frags	208	99.5	0.5	0.08	1106	0.26086	0.00124	3.3710	0.0149	0.09372	0.00019	1494.3	6.3	1497.7	3.5	1502.5	38	09
Bd-3	3 short, mbr, frags	213	75.8	0.6	0.08	1285	026224	0.00100	3.3899	0.0139	0.09375	0.00015	1501.3	6.2	1502.1	3.2	1503.1	3.1	03
Sample VP-2008: coarse dolerite sill, Kotuykan and Vurbur river areas																			
Bd-1	2 long, mbr blades	238	12.0	0.8	0.21	1012	0.25381	0.00218	3.2634	0.0333	0.09325	0.00070	1458.1	11.2	1472.4	7.9	1493.0	14.2	26
Bd-2	3 sm blade frags	107	2.6	0.4	0.04	506	0.25738	0.00269	3.2759	0.0582	0.09231	0.00120	1476.4	138	1475.3	13.8	1473.8	24.8	–0.2
Bd-4	9 short mbr blades and frags	287	9.6	0.7	0.05	835	0.30854	0.00135	3.9639	0.0370	0.09318	0.00069	1733.5	6.7	1626.8	7.6	1491.5	14.0	–18.5
Bd-5	10 short mbr blades and frags	229	12.0	1.2	0.37	632	0.22046	0.00068	2.8351	0.0322	0.09327	0.00091	1284.3	3.6	1364.9	8.5	1493.3	18.5	15.4
Bd-6	11 short mbr blades and frags	241	8.9	0.4	0 07	1430	025778	0.00093	3.3145	0.0201	0.09325	0.00042	1478.5	4.8	1484.5	4.7	1493.0	8.5	1.1
Bd-7	11 short mbr blades and frags	231	8.2	1.5	0 06	387	025770	0.00120	3.3122	0.0613	0.09322	0.00151	1478.1	6.2	1483.9	14.5	1492.3	30.8	1.1
Sample AB-87: dolerite sill, Kotuykan River																			
Bd-1	24 sm, pbr blades and frags	605	29.9	1.3	0.09	1547	0.25735	0.00049	3.3182	0.0105	0.09351	0.00021	1476.2	2.5	1485.3	2.5	1498.3	4.3	16
Bd-2	17 short + el blades and frags	706	35.2	0.9	0.10	2642	0.25832	0.00060	3.3307	0.0092	0.09351	0.00016	1481.3	3.1	1488.3	2.2	1498.3	3.2	13
Bd-3	14 sm, pbr blades	984	48.6	1.3	0.09	2529	025694	0.00049	3.3131	0.0083	0.09352	0.00014	1474.2	2.5	1484.1	2.0	1498.5	29	18
Sample AB-85: ESE dolerite dike, Kotuykan River																			
Bd-4	7 sm, pbr blades and frags	698	17.4	0.6	0.14	1798	0 25577	0.00109	3.3046	0.0178	0.09371	0.00029	1468.2	5.6	1482.1	4.2	1502.2	5.8	25
Sample AB-81: dolerite silil, Kotuykan River																			
Bd-5	9 sm, pbr blades	415	12.5	0.6	0.13	1397	0.25779	0.00086	3.3302	0.0204	0.09369	0.00043	1478.5	4.4	1488.2	4.8	1501.9	8.8	1.7

Notes. All analyzed fractions represent best quality, fresh grains of baddeleyite.

Abbreviations: Bd, baddeleyite; pbr, pale brown; mbr, medium brown; sm, small; irr, irregular/anhedral; el, elong (blade); frags, fragments.

Pb^T is total amount (in picograms) of Pb.

Pb_c is total measured common Pb (in picograms) assuming the isotopic composition of laboratory blank: 206/204—18.221; 207/204—15.612; 208/204—39.360 (errors of 2%). Pb/U atomic ratios are corrected for spike, fractionation, blank, and, where necessary, initial common Pb; $^{206}Pb/^{204}Pb$ is corrected for spike and fractionation.

Th/U is model value calculated from radiogenic $^{208}Pb/^{206}Pb$ ratio and $^{207}Pb/^{206}Pb$ age, assuming concordance.

Disc., %, Per cent discordance for the given $^{207}Pb/^{206}Pb$ age.

Uranium decay constants are from Jaffey et al. (1971).

*Analyzed at the Geological Survey of Canada (Ottawa), and reported in Ernst et al. (2000).

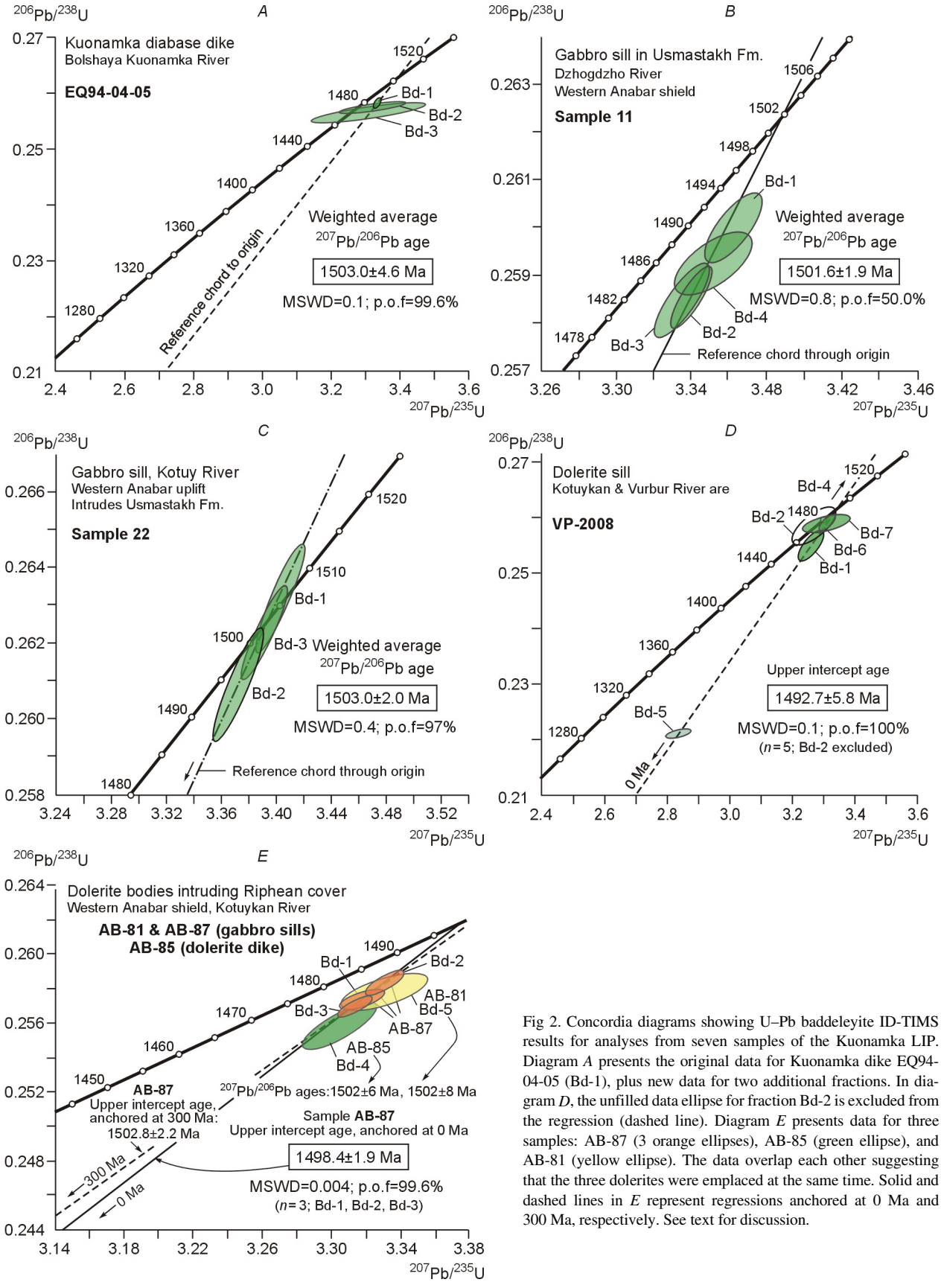

Fig 2. Concordia diagrams showing U–Pb baddeleyite ID-TIMS results for analyses from seven samples of the Kuonamka LIP. Diagram *A* presents the original data for Kuonamka dike EQ94-04-05 (Bd-1), plus new data for two additional fractions. In diagram *D*, the unfilled data ellipse for fraction Bd-2 is excluded from the regression (dashed line). Diagram *E* presents data for three samples: AB-87 (3 orange ellipses), AB-85 (green ellipse), and AB-81 (yellow ellipse). The data overlap each other suggesting that the three dolerites were emplaced at the same time. Solid and dashed lines in *E* represent regressions anchored at 0 Ma and 300 Ma, respectively. See text for discussion.

of 1493 ± 6 Ma is taken as the best estimate of the timing of emplacement and crystallization of this sill.

AB-81: Only rare baddeleyite crystals were recovered from this 30m-thick dolerite sill intruding Riphean cover along the Kotuykan River. A single U–Pb analysis of multiple baddeleyite fragments (together weighing ~0.1 micrograms) gave a $^{207}Pb/^{206}Pb$ age of 1502 ± 9 Ma (1.7% discordant), in agreement with the data obtained for AB-87 and AB-85 (see below) (Fig. 2*E*, Table 2). This preliminary age is considered a minimum estimate for the time of emplacement of this sill.

AB-85: This 50 m wide 110°-striking dolerite dike also yielded sparse baddeleyite. A single analysis of a multibaddeleyite fraction gave a $^{207}Pb/^{206}Pb$ age of 1502 ± 6 Ma (2.5% discordant), which is within analytical uncertainty of data for AB-87 and AB-81 (Fig. 2*E*, Table 2). This preliminary age is interpreted as a minimum estimate for the time of emplacement of the dike.

AB-87: U–Pb data for three baddeleyite fractions from this 25 m-thick sill overlap and indicate a small, consistent amount of Pb loss (1.2–1.8% discordant) in the grains (Fig. 2*E,* Table 2). The weighted mean $^{207}Pb/^{206}Pb$ age of 1498.4 ± 1.9 Ma ($N = 3$; MSWD = 0.004) is interpreted as a minimum age estimate for the sill. Due to the limited spread of the data, the time of Pb loss is not well defined; however, assuming a lower intercept of 300 Ma (cf. Siberian trap age of 250 Ma), increases the age to 1501.8 ± 2.2 Ma.

U–Pb baddeleyite ages for samples AB-81, AB-85, and AB-87 are equivalent and support an interpretation for synchronous emplacement of the two diabase sill samples and the one dike sample at approximately 1502 Ma, with very minor discordance dominated by recent Pb loss.

IN-SIMS geochronology

For sample F1 the date in Fig. 3 and Table 3 is based on 7 baddeleyite analyses that had greater than 99% radiogenic ^{206}Pb and Th/U less than 0.35. Two of the more discordant analyses listed in Table 3 were rejected for the age calculation based on these criteria, as these parameters are interpreted to indicate slight alteration to zircon. Six additional baddeleyite analyses were rejected that had 97 to 73 % rad ^{206}Pb and are not listed in Table 3 as these were likely highly altered baddeleyite crystals and would yield unreliable dates of magmatism. SIMS methodology followed Schmitt et al. (2010) and Chamberlain et al. (2010). Analyzed grain sizes ranged from 40 × 3 to 8 × 3 microns (see Table 3), most of them are too small to separate physically for dissolution and TIMS analysis. Discordance in SIMS U–Pb baddeleyite analyses is partly controlled by crystal orientation effects (Wingate and Compston, 2000), so the most reliable dates are based on $^{207}Pb/^{206}Pb$ data. A magmatic age of 1483 ± 17 Ma is obtained using a weighted mean of seven baddeleyite analyses.

Summary of U–Pb geochronology

The Kuonamka LIP was originally recognized in the Anabar shield where an E-trending dike was dated at 1503 ± 5 Ma (site EQ94-04), with additional E-ESE-trending dikes correlated via paleomagnetism (Ernst et al., 2000). A newly dated dike (AB85-15) with an age of 1502 ± 6 Ma extends this dike swarm into the Riphean sediments on the western slopes of the Anabar shield for a distance of 270 km. A dolerite sill province, presumably fed by this dike swarm, also cuts these Riphean sediments and yields matching ages of 1498 ± 2, 1502 ± 6, 1503 ± 2, 1502 ± 8, and 1493 ± 9 Ma (Fig. 2). A less precise age of 1483 ± 17 Ma was obtained for a sill by the U–Pb SIMS method (Fig. 3) that is within error of the TIMS dates. Several hundred kilometres farther east in the Olenek uplift (Fig. 4) a Sololi sill yielded a SHRIMP age of 1473 ± 24 Ma (Wingate et al., 2009) that is also within uncertainty of the age of the Kuonamka units farther west. Overall these data indicate that the Kuonamka LIP extends E–W for at least 700 km from the western slopes of the Anabar shield to the Olenek uplift (Fig. 4). The age of the Kuonamka LIP can be summarized as 1501 ± 3 Ma (95% confidence), based on the weighted average of the seven U–Pb ID-TIMS results.

Geochemistry

Major and trace element geochemical data (Table 4, Fig. 5) were obtained for the dated intrusions as well as for undated dikes and sills across the Anabar shield, and in intrusive rocks in the adjacent Riphean sedimentary rocks immediately west and east of the Anabar shield (Fig. 1).

The dikes and sills of the Kuonamka LIP have low MgO (4–7 wt%), SiO_2 ranging from 49% to 53%, high TiO_2 (1.5 to 3.5%). They are mainly subalkaline basalts (Figs. 6*A*, *B*) with tholeiitic character (Fig. 6*C*) and have within-plate character on trace element classification diagrams (Fig. 6*E*). On a Th/Yb vs Nb/Yb diagram (Pearce, 2008) the data plot between EMORB and OIB (closer to EMORB), and are only slightly displaced from the oceanic array indicating minimal crustal or mantle lithospheric contamination (Fig. 7). Similarly, the absence of negative Nb anomalies (Fig. 7*B*) also suggests minimal incorporation of crustal material or subduction modified lithospheric mantle (e.g., see discussion in Ernst 2014; Neumann et al., 2011).

Two geochemical groups are distinctive on most diagrams but are most obvious on a Ti vs. V diagram where Group 1 (red symbols) plot within the MORB-CFB-OFB (mid-ocean ridge, continental and oceanic flood basalt) field, while Group 2 (blue symbols) plot mostly in the oceanic island (OIB) field (Fig. 6*D*). Overall Group 2 rocks are typically more enriched (e.g., higher values for incompatible elements such as the REE and TiO_2; Figs. 7*A* and 5) than those in Group 1. Group 1 has slightly sloping LREE ($(La/Sm)_{PM}$ = 1.9) and HREE ($(Gd/Yb)_{PM}$ = 1.8), with no negative Nb anomaly, slight negative Sr and P anomalies, and moderate TiO_2 (2.2 wt%). Group 2 has slightly steeper LREE ($(La/Sm)_{PM}$ = 2.3), and HREE ($(Gd/Yb)_{PM}$ = 2.3), strong negative Sr anomaly (plagioclase fractionation) and weak negative P anomaly, is slightly higher in TiO_2 (2.7 wt%) and

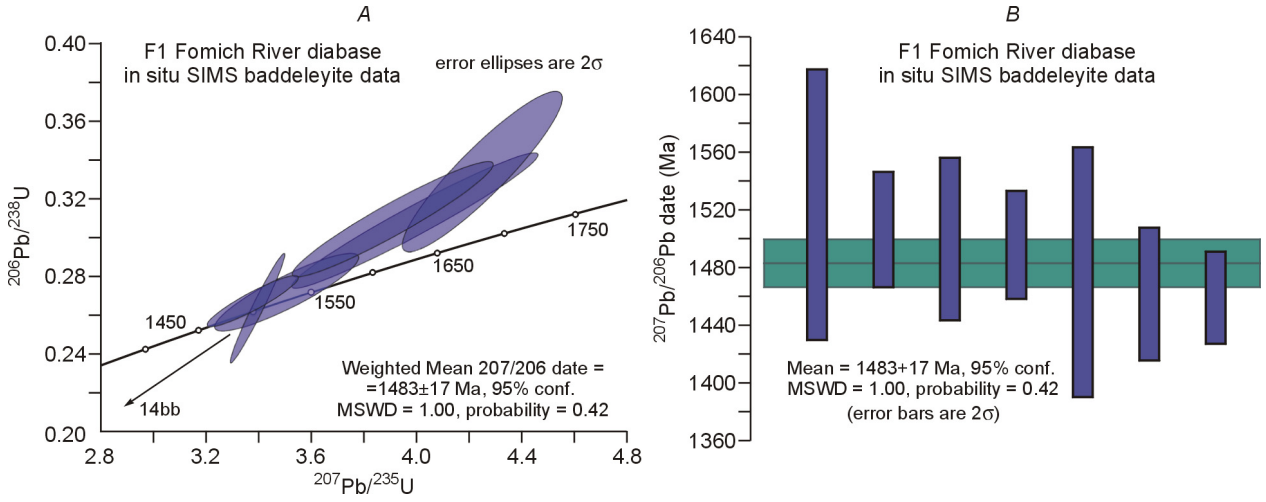

Fig. 3. U–Pb SIMS age. *A*, Concordia plot of all 7 analyses with radiogenic ^{206}Pb greater than 99% and Th/U less than 0.35. Grain sizes ranged from 8 to 40 microns in length, 3 to 10 microns in width. Data come from in-situ SIMS analyses. *B*, Weighted mean $^{207}Pb/^{206}Pb$ date of baddeleyite in-situ SIMS analyses.

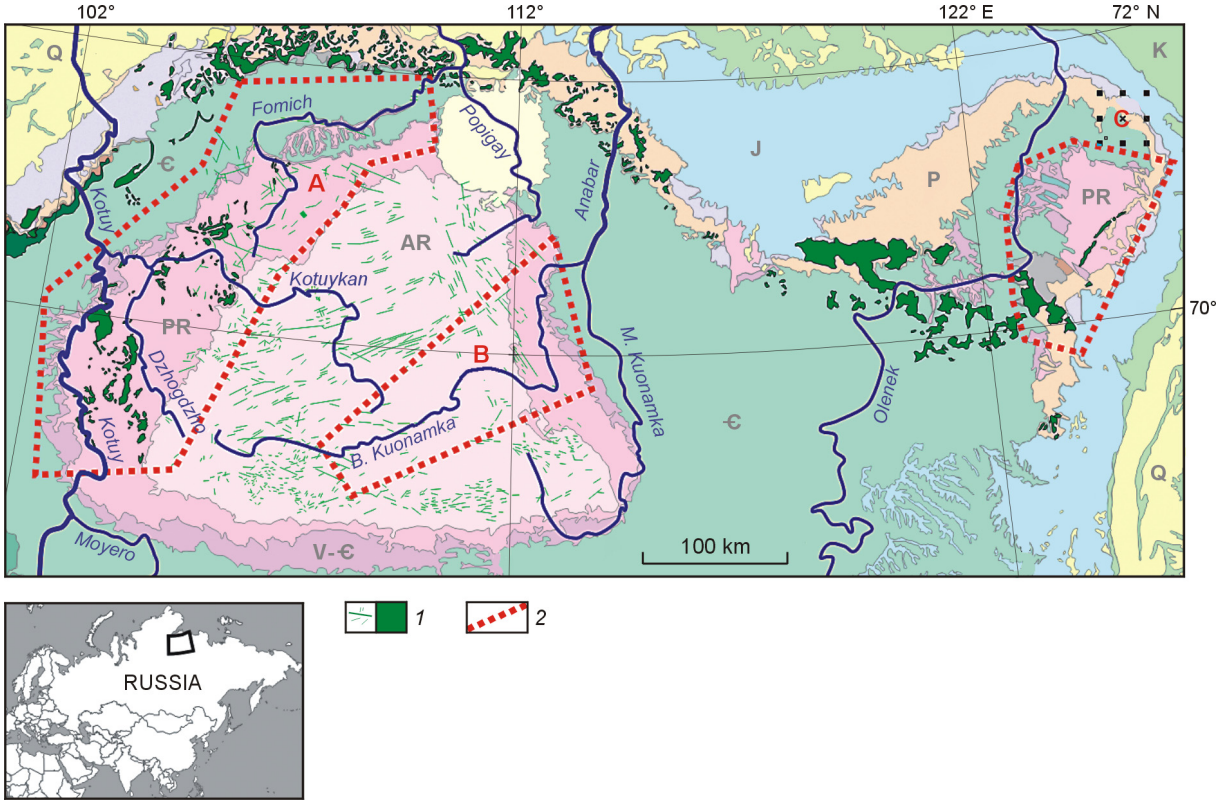

Fig. 4. Regional distribution of confirmed units belonging to the Kuonamka LIP. Area A is on the Riphean sedimentary packages on the western slopes of the Anabar uplift, Area B is within the basement rocks of the Anabar Shield and into the eastern Riphean cover and Area C is within the Olenek uplift. Additional study is expected to reveal additional units of the Kuonamka LIP throughout the Anabar shield and surrounding areas covered by Riphean (Proterozoic) cover rocks, such as between and around areas A and B. Kuonamka units likely extend at depth throughout the region beneath younger cover rocks. AR, Archean; PR, Proterozoic; V–Є, Vendian–Cambrian; Є, Cambrian; P, Permian; K, Cretaceous; J, Jurassic; Q, Quaternary. *1*, dikes and sills of different ages; *2*, Kuonamka LIP areas.

other incompatible elements, and is transitional to alkaline in composition (Fig. 6*A*, *B*).

Depth of melting may have played a role in establishing geochemical differences expressed between Group 1 and 2 compositions. Higher $(Gd/Yb)_{PM}$ ratios in some Group 2 samples could indicate that melting occurred partly within the garnet stability zone of the mantle (Gd/Yb_{PM} >2), whereas the lower $(Gd/Yb)_{PM}$ ratios evident in most Group 1 samples may have been inherited from dominantly shallower depth of melting (e.g., spinel stability field) (Fig. 6*F*).

Table 3. SIMS data from in-situ analyses of baddeleyite

Sample	Grain size (μm)	Ages (Ma)						r206Pb, %	Ratios					UO_2/U	U, ppm	Th/U
		$^{206}Pb/^{238}U$	1 s.e.	$^{207}Pb/^{235}U$	1 s.e.	$^{207}Pb/^{206}Pb$	1 s.e.		$^{206}Pb^*/^{238}U$	1 s.e., %	$^{207}Pb/^{235}U$	1 s.e., %	rho			
F1	1483 ± 17 Ma, 95% conf. 7 point weighted mean $^{207}Pb/^{206}Pb$ date (MSWD = 1.00, prob. = 0.42)															
grain 14b	10 × 6	390	(11)	605	(16)	1523	(47)	99.3	0.062	(2.8)	0.815	(3.6)	0.73	11.10	257	0.27
grain 6b	8 × 3	1734	(70)	1633	(39)	1506	(20)	99.1	0.309	(4.6)	3.995	(4.8)	0.97	6.74	240	0.28
grain 14e	8 × 3	1549	(42)	1529	(26)	1500	(28)	99.5	0.272	(30)	3.506	(3.2)	0.89	9.19	243	0.15
grain 16"	15 × 10	1508	(58)	1503	(35)	1496	(19)	99.7	0.264	(4.3)	3.394	(1.3)	0.98	11.80	182	0.10
grain 36"	30 × 6	1855	(81)	1684	(46)	1477	(43)	99.3	0.334	(5.0)	4.251	(2.9)	0.91	10.90	378	0.30
grain 6a	8 × 3	1737	(59)	1616	(33)	1462	(23)	99.4	0.309	(3.9)	3.910	(4.0)	0.95	7.61	240	0.28
grain 9	10 × 5	1527	(27)	1499	(17)	1459	(16)	99.8	0.267	(2.0)	3.376	(2.1)	0.92	12.50	206	0.27
grain 20°	40 × 3	1462	(27)	1449	(17)	1431	(15)	99.5	0.255	(2.1)	3.167	(2.2)	0.94	11.30	599	0.41
grain 14a°	30 × 3	781	(19)	949	(31)	1363	(80)	98.2	0.129	(2.6)	1.547	(5.0)	0.56	11.20	152	0.17

Note. Values in parentheses are absolute errors at one sigma level for ages, percent for ratios. r206Pb = radiogenic ^{206}Pb in percent; * = radiogenic Pb value corrected for initial Pb; rho = correlation coefficient of error ellipses; ° = excludeci from age calculation due to high Th/U or low % r206Pb.
Data acquired January 31,2008 (") and January 25, 2012 on the CAMECA *ims* 1270 secondary ion microprobe (SIMS) at UCLA (University of California at Los Angeles), USA. Microbaddeleyite grains were analyzed in-situ from polished thin sections using an aperture in the transfer section of the secondary beam column to reduce the effective sampling diameter from 20 microns to approximately 8 microns. Sample chamber was flooded with oxygen (~105 Torn) to enhance Pb secondary ion yields for baddeleyite by approximately 10-fold; U/Pb relative sensitivity was calibrated by UO_2/U. Phalaborwa baddeleyite standard analyzed during the same session yielded a weighted mean $^{207}Pb/^{206}Pb$ date of 2060.4 ± 3.4 Ma (95% confidence, MSWD 1.5), $^{206}Pb/^{238}U$ date of 2031 ± 44 Ma (MSWD 0.52) and UO_2/U from 7.69 to 9.61. Pb values were corrected for common Pb using the ^{204}Pb method.

Discussion

On the basis of the U–Pb dating and geochemical characterisation described above, some additional aspects of the nature of this Kuonamka LIP have become evident.

Age distribution of Group 1 and Group 2 magmas

Six of the U–Pb ages determined are associated with Group 1 magmatism, and five of these (all ID-TIMS ages) are consistent with a narrow interval of emplacement between 1498-1503 Ma (Table 1). Given its closely matching chemistry, the Fomich River sill sample (F-1) with the less precise U–Pb SIMS age of 1483 ± 17 Ma may be included with Group 1 samples. Only one sample from Group 2 (sample #11) is dated (1502 Ma) and has some geochemical characteristics transitional to Group 1. Thus the precise age of Group 2 is not yet known but on the basis of its steeper HREE pattern (for 3 of its 5 samples) could slightly precede Group 1 magmatism if the magma is being generated in a plume; in such a case the Group 2 magma could represent deeper (earlier) melting in an ascending mantle plume.

Geographic distribution of Group 1 and Group 2 magmas

Given the geochemical and precise U–Pb results presented herein, a tantalizing question is whether the distributions of Group 1 and 2 magmas show any spatial pattern that provides insight into the LIP plumbing system. For instance, in some LIP events, there is a tendency for lower Ti magma type to be located in the plume centre region where there is predicted to be a higher degree of partial melting. If there is a difference in timing of emplacement between the two groups (e.g., Group 2 earlier than Group 1) then, depending on the magnitude of the time gap and any stress changes during that interval, there may be some differences in distribution. A sill province may show compositional difference as a function of depth, with potential filling from lower levels upward. However, the plumbing system of LIPs can be more complicated. For instance, adjacent sills belonging to the Karoo LIP can represent different magma batches and more distal sills can belong to the same magma batch (e.g., Fig. 10 in Neumann et al., 2011). In any case, it is noted here (Fig. 9) that the sites with Group 1 and Group 2 chemistry are spatially intermixed.

Location of mantle source

As discussed above the geochemical results (Figs. 5–8) clearly show that crustal input (from continental crust or metasomatized lithospheric mantle) into the Kuonamka magmas is minor, which is unexpecteed given that they are cutting continental crust in the interior of the Siberian craton. Furthermore, their compositions (especially of Group 1) indicate a depth of melt generation that is generally shallower than the garnet stability field in the mantle, i.e., less than about 75 km. The Siberian craton, and in particular this region, has seismic tomography information that indicates a lithospheric root extending to ~250 km (Rosen et al., 2005) and even to 300 km (Kuskov et al., 2011), i.e., deeper than the depth of melt generation for the majority of Kuonamka magmas. Thus the magmas were not generated in the mantle immediately beneath this northern portion of the Siberian craton. This paradox is resolved by considering that major dolerite dike swarms can transport magma laterally into the crust from

Table 4. Geochemistry data belonging to the Kuonamka LIP

Component	EQ94-01-01	EQ94-04-05	EQ94-02-05	AB85-15	AB87-11	AB81-2	139-153	81-108	14	24
Group 1										
SiO_2, wt%	51.09	52.96	50.25	50.22	51.20	50.91	50.51	50.98	51.47	51.18
TiO_2	2.28	1.75	2.18	2.69	2.53	1.95	2.01	2.02	1.97	2.92
Al_2O_3	13.82	12.75	14.22	13.67	13.74	13.76	13.68	13.29	13.70	12.56
FeO^T	12.53	14.35	12.47	14.44	14.20	12.66	12.31	12.70	13.69	16.43
MnO	0.20	0.22	0.18	0.21	0.21	0.19	0.16	0.18	0.22	0.24
MgO	6.48	5.35	7.27	5.55	5.19	6.85	7.16	7.44	6.14	4.22
CaO	10.40	9.71	10.45	8.99	8.14	9.75	10.07	9.71	9.54	8.57
Na_2O	2.38	2.29	2.33	2.28	2.13	2.16	2.25	1.95	2.30	2.84
K_2O	0.57	0.45	0.43	1.72	2.42	1.59	1.64	1.52	0.77	0.78
P_2O_5	0.25	0.17	0.21	0.23	0.24	0.18	0.22	0.22	0.21	0.26
LOI	1.84	1.24	1.12	1.58	1.97	1.52	1.65	1.19	1.83	1.65
Ba, ppm	207	206	192.5	176	244	117	168.5	195.5	208	231
Ce	43.3	40.2	37.7	37.4	43	31.3	36.8	39	35.5	46.7
Co	45	51	49	48	42	45	46	49	51	52
Cr	120	40	130	30	30	130	160	120	90	10
Cs	0.18	0.08	0.07	0.31	0.56	0.14	0.32	0.31	0.19	0.19
Cu	173	189	165	198	214	107	135	136	161	218
Dy	5.37	5.27	4.78	5.47	6.46	4.78	5.27	5.45	5.21	6.86
Er	2.93	3.16	2.87	2.98	3.5	2.78	2.86	3.1	2.89	3.85
Eu	1.97	1.84	1.82	1.93	2.2	1.67	1.73	1.95	1.71	2.08
Ga	20.3	19.9	20.9	21.2	21.9	19.1	19.2	20.4	19.3	22.4
Gd	6.17	5.65	5.72	5.99	6.75	5.02	5.67	5.74	5.41	7.23
Hf	4.6	4.2	4.1	4.2	4.5	3.6	3.8	4.3	3.9	5.3
Ho	1.04	1.17	1.03	1.13	1.28	0.97	1.02	1.1	1.14	1.4
La	18.5	17.4	15.8	15.7	17.9	13.1	15.6	16.4	16.4	21.8
Lu	0.37	0.41	0.33	0.37	0.44	0.31	0.35	0.41	0.42	0.53
Nb	15.5	12.9	17.5	14.7	16.1	11.5	12.9	13.8	11.5	16.2
Nd	26	23.2	23	22.6	26	19.4	22.4	23.3	21.8	28.5
Ni	106	62	137	60	45	94	109	130	79	37
Pb	<2	2	2	<2	<2	<2	<2	3	6	4
Pr	6	5.56	5.25	5.26	5.98	4.3	5.28	5.48	4.83	6.32
Rb	12	8.8	7.3	25.4	41.6	21.1	33.9	23.2	14.3	15.7
Sc	29	37	29	30	31	32	30	29	35	38
Sm	5.98	5.8	5.53	5.55	6.4	4.81	5.36	5.81	5.31	7.03
Sr	294	203	344	282	326	244	353	284	230	207
Ta	0.8	0.8	0.8	0.8	0.9	0.7	0.8	0.8	0.7	1
Tb	0.99	0.97	0.83	0.94	1.13	0.86	0.96	0.92	0.9	1.12
Th	2.13	2.32	1.81	1.71	1.94	1.52	1.77	2	1.86	2.49
Ti	13,676	10,520	13,076	16,141	15,158	11,662	12,025	12,087	11,804	17,504
Tm	0.41	0.47	0.39	0.41	0.52	0.4	0.41	0.44	0.43	0.55
U	0.5	0.53	0.39	0.38	0.48	0.38	0.44	0.45	0.43	0.56
V	348	427	369	470	420	355	346	358	347	497
Y	26.1	28.8	24.4	26.7	31.5	24.4	25.3	27.2	27.2	35.8
Yb	2.49	3.1	2.47	2.77	3.43	2.36	2.39	2.65	2.76	3.52
Zn	119	123	117	126	111	82	96	107	117	151
Zr	170	158	154	154	174	135	149	163	146	197

(*continued on next page*)

Table 4 (*continued*)

Component	EQ94-13-01	EQ94-14-02	EQ94-03-05	259-273	215-225	11
Group 2						
SiO_2, wt%	52.18	50.67	49.97	52.29	52.55	51.97
TiO_2	3.48	3.40	3.09	3.62	3.53	2.53
Al_2O_3	12.89	13.14	13.60	11.90	11.91	14.01
FeO^T	13.25	14.06	13.62	15.96	15.96	13.71
MnO	0.15	0.20	0.21	0.23	0.24	0.18
MgO	5.66	4.84	5.83	3.90	3.87	7.22
CaO	7.38	7.63	9.48	6.42	6.38	4.01
Na_2O	2.65	2.35	2.67	3.39	3.32	3.54
K_2O	1.50	2.90	0.92	1.87	1.81	2.53
P_2O_5	0.88	0.82	0.62	0.42	0.43	0.30
LOI	3	1.79	1.52	1.9	1.8	4.7
Ba, ppm	495	556	380	372	302	407
Ce	101	96.6	72.3	72.7	72.3	59.4
Co	33	41	42	39	40	46
Cr	50	50	90	10	10	20
Cs	0.53	0.4	0.11	0.22	0.28	0.19
Cu	53	52	84	129	153	82
Dy	9.75	9.41	7.15	8.61	9.01	4.89
Er	4.89	4.58	3.51	4.88	4.77	2.47
Eu	4.53	4.17	3.33	3.21	3.05	2.09
Ga	25.1	25.1	22.9	22.8	23.7	19.6
Gd	12.45	11.35	9.14	10.05	9.92	6.33
Hf	8	8.1	6	7.5	7.8	5.3
Ho	1.86	1.81	1.39	1.7	1.8	0.92
La	42.3	40.8	30.2	31.5	30.9	26.2
Lu	0.51	0.55	0.45	0.59	0.59	0.3
Nb	32	31.2	24.1	26.8	26.8	19.5
Nd	59.6	56.3	42.6	42.3	43.2	31
Ni	41	44	89	4	5	48
Pb	3	<2	7	7	<2	3
Pr	13.95	13.35	10.1	9.83	9.95	7.72
Rb	30.5	54	18.1	34.4	36.2	30.6
Sc	24	23	25	30	30	21
Sm	13.85	12.7	9.92	9.68	9.91	6.54
Sr	405	451	466	190	219	97.7
Ta	2	1.9	1.5	1.7	1.6	1.2
Tb	1.86	1.79	1.35	1.58	1.57	0.91
Th	4.42	4.25	3.18	3.47	3.47	3.37
Ti	20,853	20,356	18,516	21,710	21,147	15,192
Tm	0.66	0.58	0.48	0.67	0.67	0.32
U	1.04	0.98	0.83	0.81	0.85	0.77
V	305	316	332	275	262	313
Y	45	43	34.2	43.1	43.9	21.7
Yb	4.12	3.74	3.02	4.12	4.48	2.16
Zn	199	161	161	184	127	142
Zr	322	314	233	294	298	210

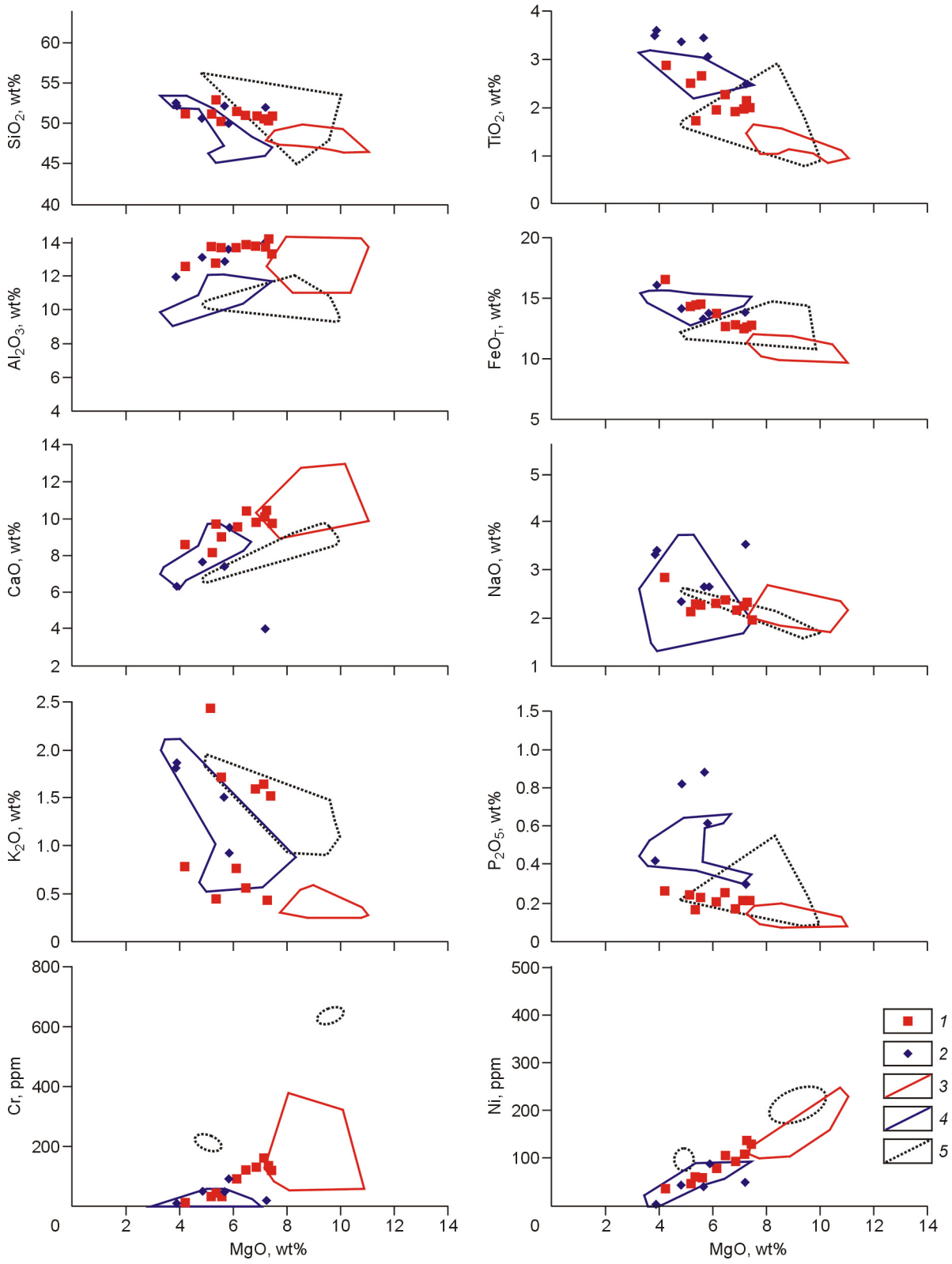

Fig. 5. Selected elements plotted against MgO. FeO_T represents total iron calculated as FeO. *1*, Group 1; *2*, Group 2; *3*, Chapada Diamantina dikes; *4*, Curaçá dikes; *5*, Angola sills and dikes.

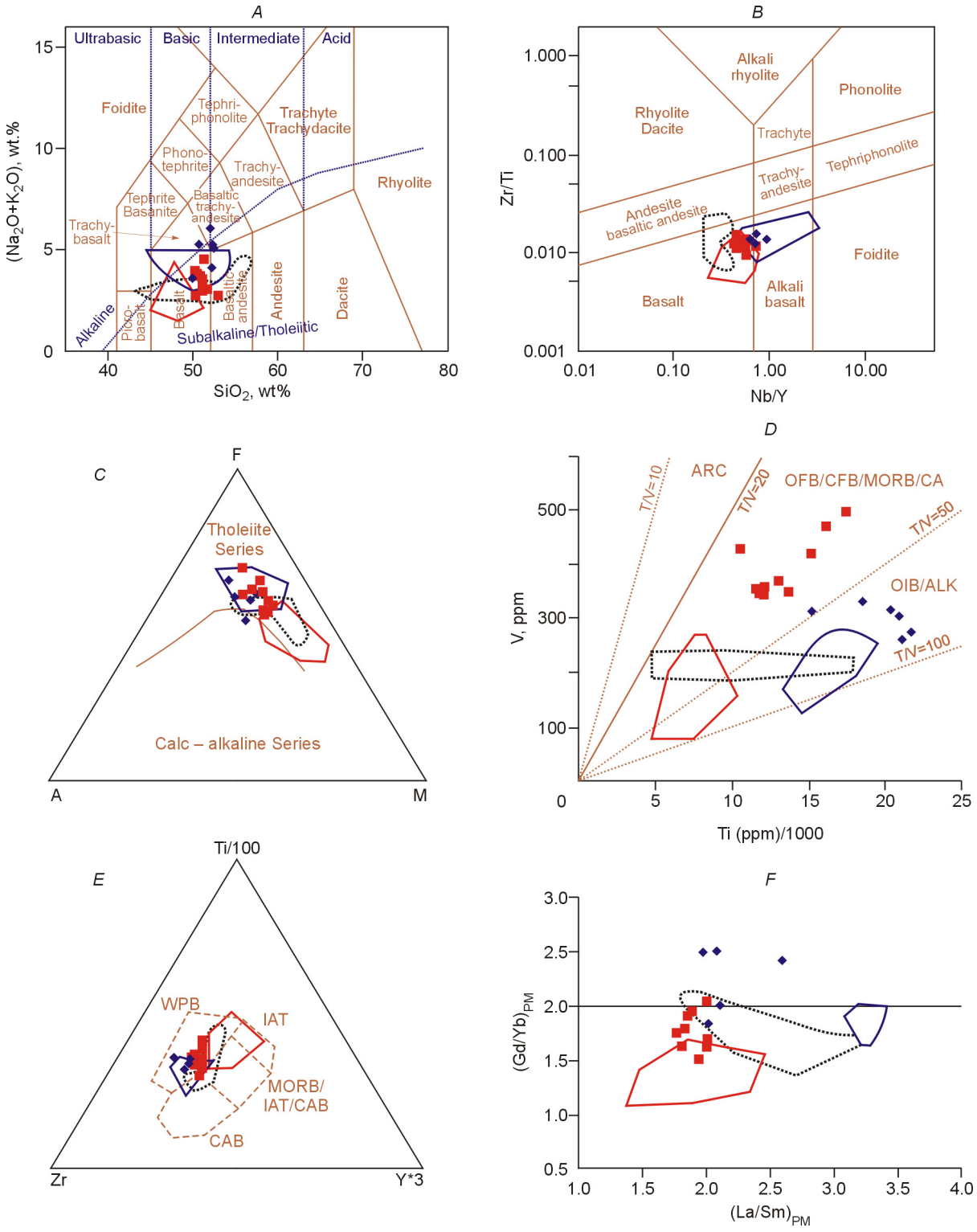

Fig. 6. Selected geochemical diagrams for mafic dikes and sills of the Kuonamka LIP—Group 1 (red squares) and Group 2 (blue diamonds). For comparison, fields of data are also shown for age-equivalent mafic intrusive units from the São Francisco craton (SFC): Chapada Diamantina (red line) and Curaçá dikes (blue line), as well as from the Angola block of the Congo craton (dotted outline) (see Discussion section). *A*, Total alkalis-silica (TAS) diagram; *B*, trace element proxy for TAS diagram, after Winchester and Floyd (1977), as modified by Pearce (1996); *C*, AFM diagram (Irvine and Baragar, 1971); *D*, V vs. Ti diagram of Shervais (1982). ARC, Arc tholeiites; OFB, oceanic flood basalt; CFB, continental flood basalt; MORB, mid-ocean ridge basalt; CA, calc-alkaline basalt; OIB, oceanic island basalts; ALK, alkaline basalt; *E*, tectonic setting classification diagram of Pearce and Cann (1973); WPB, within-plate basalts; IAT, island arc tholeiites; CAB, calc alkaline basalts; *F*, Heavy REE slope (Gd/Yb) vs. Light REE slope (La/Sm). The SFC data and Angola data are addressed in the Discussion section. The horizontal line in part F represent the heavy REE slope; values of $(Gd/Yb)_{PM} > 2$ indicate melt generation in the garnet stability field (~>75 km).

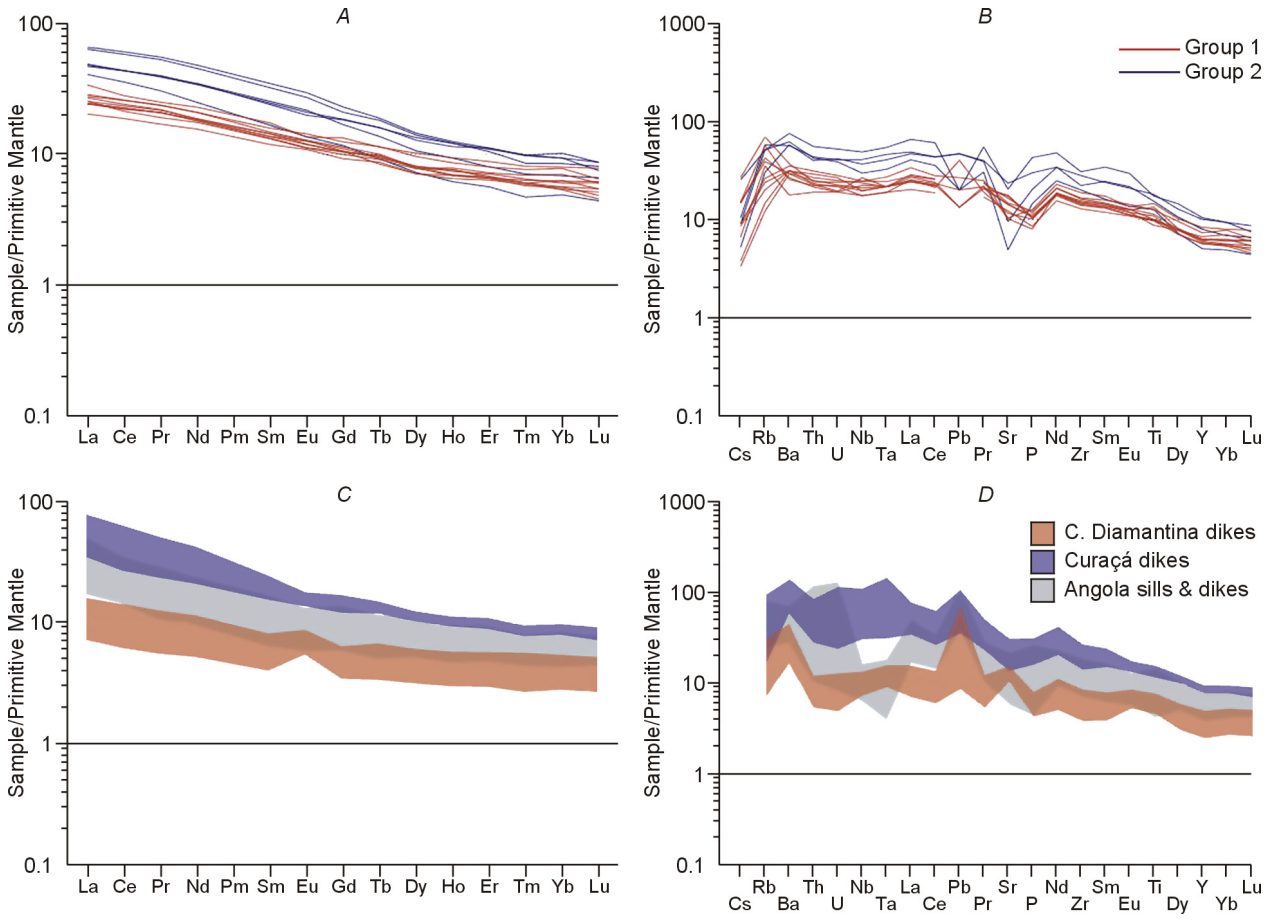

Fig. 7. Rare earth (REE) and incompatible trace element diagrams for the Kuonamka suites (Groups 1 and 2) in parts *A* and *B*, and for dolerite dikes and sills of the same age in the São Francisco craton (SFC) and Congo craton (Angola block) in parts *C* and *D*. The SFC and Angola data are addressed in the Discussion section.

source areas at the edges of cratons (e.g., Ernst, 2014). If this applies to the Kuonamka dikes then we can use the trend of the dike swarm to indicate which margins of the Siberian craton were overlying potential mantle source areas at that time. The trend of both Group 1 and Group 2 Kuonamka dikes magmas is mainly E to ESE and extrapolating the trend of the dikes to the edge of the Siberian craton would locate thinner lithosphere where the requisite partial melting could occur. Thus the source area (presumably marked by a mantle plume) could be either to the northeastern or northwestern sides of the Siberian craton (Fig. 10).

Reconstruction with combined São Francisco–Congo cratons

Here we consider a match with coeval dikes and sills in the combined São Francisco craton and Congo craton. In the SFC the Chapada Diamantina and Curaça dike swarms yield U–Pb baddeleyite ages of 1503 ± 7 Ma and 1508 ± 3 Ma, respectively (Silveira et al., 2013). In addition, as summarized in Figueiredo et al. (2009), Babinsky et al. (1999) gives a U–Pb age of 1514 ± 22 Ma on zircon from a gabbro sill, Battilani et al. (2005) provides a similar Ar–Ar age on a dike, and Guimarães et al. (2005) presents a U–Pb age of 1496 ±

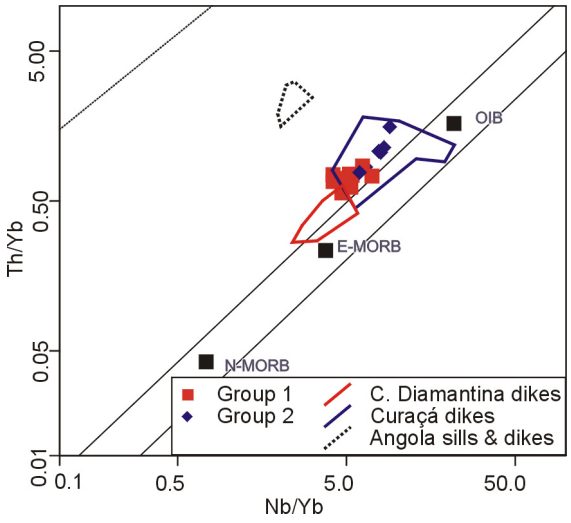

Fig. 8. Data plotted on diagrams from Pearce (2008). The red squares and blue diamonds correspond to Groups 1 and 2 rocks, respectively. The meaning of SFC data (red and blue outlined fields) and Angola data (dotted black outline) are addressed in the Discussion section. The Kuonamka data (Group 1 and Group 2) and SFC data (Chapada Diamantina and Curaçá dikes) are interpreted as mantle melts (with composition between E-MORB and OIB) with only minor contamination by continental crust or metasomatized lithospheric mantle. In contrast the Angola data (from the Congo craton) exhibits significant contamination.

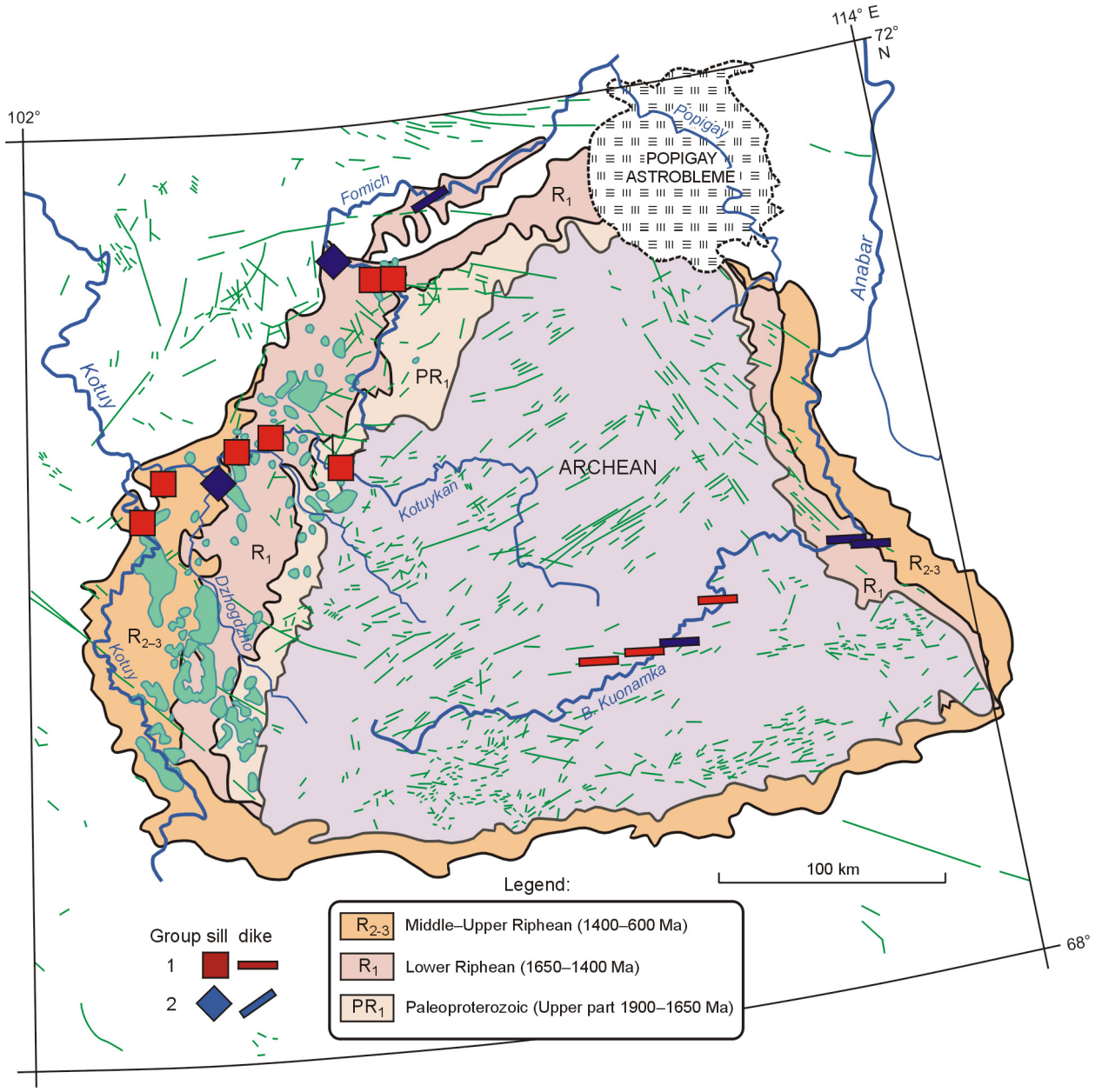

Fig. 9: Distribution of Groups 1 (red square symbols) and 2 (blue diamond symbols) dikes and sills. Base map is the same as for Fig. 1.

3 Ma on zircon from a gabbro intruding into the uppermost unit of the Chapada Diamantina sequence. Hence, it can be inferred that the ca. 1500 Ma event represents a significant barcode 'line' for the São Francisco craton. In addition, recent evidence presented in Ernst et al. (2013b) has demonstrated an equivalent age of prominent mafic magmatism in the Angolan portion of the Congo craton in central Africa (Humpata dolerite sill; 1502 ± 5 Ma, U–Pb TIMS, baddeleyite).

The São Francisco and Congo cratons are presumed to have been connected from at least 2.0 Ga until their ca. 130 Ma breakup during opening of the South Atlantic (D'Agrella-Filho et al., 1996; Feybesse et al., 1998). Thus, the 1503–1508 Ma Chapada Diamantina and Curaça dikes of the SFC and the 1502 Ma Humpata sills of Congo craton represent a single magmatic province, which can be correlated temporally with the 1501 Ma Kuonamka dike and sill province and is consistent with available paleomagnetic data. Specifically, Ernst et al. (2013b) proposed that the eastern side of the combined SFC–Congo craton was attached to northern Siberia at ca. 1500 Ma. Cederberg et al. (2016) juxtapose Siberia and SFC–Congo in a different configuration. However, in either geometry (Fig. 10*A*, *B*) the greatly expanded scale of the Kuonamka LIP (determined by the U–Pb dating herein), when combined with the coeval Curaçá–Chapada Diamantina and Humpata magmatism of SFC and Congo cratons, respectively, results in a single, short duration, high-volume 1501 ± 3 Ma LIP event that is over 2000 km across, and therefore represents a particularly large LIP event (e.g., Ernst, 2014).

Comparison with the 1505 Ma dikes of the SFC

If, as inferred above, the 1500 Ma SFC and Congo (Angola block) magmatism belongs to the Kuonamka LIP then a geochemical comparison would be illuminating. In some LIPs it is observed that most portions of a given event have similar geochemical characteristics and often carry characteristic, normalized incompatible trace element abundance patterns. Examples include the 510 Ma Kalkarindji LIP of Australia (e.g., Evins et al., 2009), and the 780 Ma Gunbarrel LIP of Western North America (e.g., Sandeman et al., 2014). However, in other LIPs a range of compositional groups can be observed. For instance, the volcanic rocks of the Siberian Trap LIP are divided into a number of chemostratigraphic groups (e.g., Lightfoot et al., 1994) despite the overall duration of magmatism being less than about 1 million years (Burgess and Bowring, 2015). In such cases, multiple mantle source regions may have been involved, separate plumbing systems could have been exploited, and varied crustal contamination scenarios must be considered.

Lithogeochemical data for the Chapada–Diamantina and Curaçá dikes of the SFC were reported by Silveira et al. (2013). The data from the Chapada–Diamantina and Curaçá dikes were recognized to fall into two groups, with the Curaçá dikes having a slight alkaline chemistry (Silveira et al., 2013). In comparison with the Kuonamka dikes, it can be seen that there is a correlation between Group 2 (Kuonamka) and Curaçá data, while Group 1 (Kuonamka) data tend to continue the trends of Chapada Diamantina data. In addition, all the groups lack a significant negative Nb anomaly confirming the absence of any subduction component (Figs. 6–8). Sr and Nd isotopic data (in progress) will help better constrain the petrogenetic history of Group 1 and Group 2 of the Kuonamka LIP.

Comparison with the 1500 Ma Humpata sills and dikes from the Congo craton

Geochemically, the Humpata craton sills and dikes from the Angola block of the Congo craton (Ernst et al., 2013b) mostly overlap compositionally with the Kuonamka and SFC dike and sill data, but also show some differences (Figs. 5–8). Where the Congo (Humpata) data most dramatically differ is having a negative Nb anomaly, suggesting input of a subduction component into the magmatism. Provided there are no analytical biases arising from the use of different analytical laboratories, the Humpata sills and dikes appear to represent a different magma batch that has evolved separately from the Kuonamka dikes and sills, and the Chapada Diamantina and Curaçá dikes of the São Francisco craton. The differences between the Humpata units and the rest of Kuonamka LIP are amplified by the observation that the Humpata sills have olivine (Ernst et al., 2013b) whereas none is observed in the Kuonamka samples (e.g., Ernst et al., 2000). Provisionally, the 1500 Ma Humpata magmatism represents a distinct magmatic suite in the Kuonamka LIP but further geochemistry and isotopic work is required to better characterize the relationship with the rest of the Kuonamka LIP.

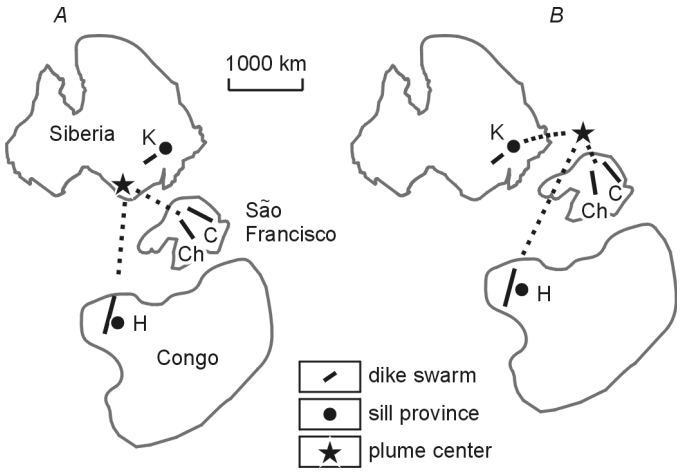

Fig. 10. 1500 Ma magmatism superimposed on two alternative reconstruction of northern Siberia with the combined São Francisco–Congo craton. *A*, Modified from Ernst et al. (2013b) with the interpreted plume located east of the Siberian craton; *B*, modified from Cederberg et al. (2016) with the interpreted plume located to the west of the Siberian craton. K, Kuonamka dikes and sill; C, Curaçá; Ch, Chapada Diamantina dikes; H, Humpata sills and dikes.

Conclusions

A combination of ID-TIMS and *in situ* ion probe (SIMS) U–Pb dating of baddeleyite from several mafic (dolerite) dikes and sills across northern Siberia has revealed the presence of a large igneous province dated at approximately 1501 ± 3 Ma. This regionally significant event spans approximately 700 km, from the western flanks of the Anabar shield eastward to the Olenok uplift. Geochemical data indicate fractionated, iron-enriched magmas that were dominantly tholeiitic basalt in composition with relatively low MgO (4–7 wt%) and within-plate character based on trace element classification diagrams. The data plot between E-MORB and OIB and on the basis of multiple geochemical criteria, crustal input to these mantle-derived magmas appears to have been minor (based on Figs. 6*F* and 8*A*). Two geochemical subgroups are distinguished: Group 2 is more enriched (with higher REE and TiO_2 concentrations) than Group 1 and typically has a greater heavy REE slope indicating some melting at depths greater than 75 km (in the garnet stability field). Group 2 has composition closer to OIB and to the alkaline field. The two geochemical subgroups overlap in geographic distribution and ages, and are probably related pulses in a single LIP.

Proposed reconstructions of the Kuonamka LIP with 1500 Ma magmatism of the SFC–Congo craton are supported by a geochemical comparison. Specifically, the chemistry of the Chapada Diamantina and Curaçá dikes of the SFC are linked to Groups 1 and 2, respectively, of the Kuonamka LIP. This reconstructed event, consisting of Kuonamka dikes and sills (of northern Siberia), the Chapada Diamantina and Curaçá dikes of the SFC and the Humpata sills and dikes of the Congo craton define a major LIP that extends at least 2000 km in diameter.

Acknowledgments. The authors would like to thank undergraduate students Celeste Vatcher, Etienne Menard and Ronan Drysdale, for their help with geochemical sample preparation. Sandra Kamo and Mike. Hamilton acknowledge the skilled help of Kim Kwok and Boris Foursenko in the Jack Satterly Lab (U. Toronto). This is publication number 57 of the 2010–2015 LIPs—Supercontinent Reconstruction—Resource Exploration Project (www.supercontinent.org; www.camiro.org/exploration/ongoing-projects). Vladimir Pavlov and Roman Veselovskiy were partly supported by Grants RFBR #13-05-12030 and #15-35-20599, Ministry of Education and Science of the Russian Federation Grant #14.Z50.31.0017. Reviews by Andrei Izokh and Mikhail Kuzmin are greatly appreciated.

References

Babinsky, M., Pedreira, A.J., Brito Neves, B.B., Van Scmus, W.R., 1999. Contribuição à Geochronologia da Chapada Diamantina. VII Simposio Nacional de Estudos Tectonicôs, Lençois, pp. 118–120.

Battilani, G.B., Vasconcellos, P.M., Gomes, N.S., Guerra, W.J., 2005. Geochronological data of dikes and sills intruding Proterozoic sequences of the Tombador Formation, Bahia, Brazil, in: Anais III Simpósio sobre o Cráton do São Francisco (Symposium on the São Francisco Craton). CBPM/SBG/UFBA, Salvador-BA, pp. 139–142.

Burgess, S.D., Bowring, S.A., 2015. High-precision geochronology confirms voluminous magmatism before, during, and after Earth's most severe extinction. Science Advances 1 (7), e1500470, doi: 10.1126/sciadv.1500470.

Cederberg, J., U. Söderlund, U., Oliveira, E.P., Ernst, R.E., Pisarevsky, S.A., 2016. U–Pb baddeleyite dating of the Proterozoic Pará de Minas dike swarm in the São Francisco craton (Brazil)—implications for tectonic correlation with Siberia, Congo and the North China cratons *GFF* (in press).

Chamberlain, K.R., Schmitt, A.K., Swapp, S.M., Harrison, T.M., Swoboda-Colberg, N., Bleeker, W., Peterson, T.D., Jefferson, C.W., Khudoley, A.K., 2010. In-situ U–Pb SIMS (IN-SIMS) micro-baddeleyite dating of mafic rocks: method with examples. Precambrian Res. 183, 379–387. doi: 10.1016/j.precamres.2010.05.004.

D'Agrella Filho, M.S., Feybesse, J.L., Prian, J.P., Dupuis, D., N'Dong, J.E., 1996. Paleomagnetism of Precambrian rocks from Gabon, Congo craton, Africa. J. African Earth Sciences 22, 65–80.

Ernst, R.E., 2014. Large Igneous Provinces. Cambridge University Press.

Ernst, R.E., Buchan, K.L., Hamilton, M.A., Okrugin, A.V., Tomshin, M.D., 2000. Integrated paleomagnetism and U–Pb geochronology of mafic dikes of the Eastern Anabar shield region, Siberia: implications for Mesoproterozoic paleolatitude of Siberia and comparison with Laurentia. J. Geol. 108, 381–401.

Ernst, R.E., Hanes, J.A., Puchkov, V.N., Okrugin, A.V., Archibald, D.A., 2008. Reconnaissance Ar–Ar dating of Proterozoic dolerite dikes and sills in Siberia and the southern Urals: identification of possible new Large Igneous Provinces (LIPs), in: Common and Regional Problems of Tectonics and Geodynamics, Moscow Tectonics Conference, Extended Abstract. GEOS, Moscow, pp. 492–496.

Ernst, R.E., Bleeker, W., Soderlund, U., Kerr, A.C., 2013a. Large Igneous Provinces and supercontinents: Toward completing the plate tectonic revolution. Lithos 174, 1–14.

Ernst, R.E., Pereira, E., Hamilton, M.A., Pisarevsky, S.A., Rodriques, J., Tassinari, C.C.G., Teixeira, W., Van-Dunem, V., 2013b. Mesoproterozoic intraplate magmatic "barcode" record of the Angola portion of the Congo craton: newly dated magmatic events at 1500 and 1110 Ma and implications for Nuna supercontinent reconstructions. Precambrian Res. 230, 103–118.

Ernst, R.E., Hamilton, M.A., Kamo, S.L., Okrugin, A.V., Veselovskiy, R.V., Pavlov, V., Söderlund, U., Chamberlain, K.R., 2014. The 1498–1503 Ma Kuonamka LIP of northern Siberia; new precise U–Pb baddeleyite dating. GAC-MAC annual meeting, Fredericton, New Brunswick, Canada, May 21–23.

Ernst, R.E., Söderlund, U., Hamilton, M.A., Chamberlain, K.R., Bleeker, W., Okrugin, A.V., LeCheminant, A.N., Kolotilina, T., Mekhonoshin, A.S., Buchan, K.L., Gladkochub, D.P., Didenko, A.N., Hanes, J.A., 2015. Long term neighbors: Reconstruction of southern Siberia and northern Laurentia based on multiple LIP barcode matches over the interval 1.9–0.7 Ga. Irkutsk. Keynote Presentation, in: Large Igneous Provinces, Mantle Plumes and Metallogeny in the Earth's History (International Conference) 1–8 September Irkutsk–Listvyanka, Siberia, Russia. http://lip2015.igc.irk.ru/.

Ernst, R.E., Hamilton, M.A., Söderlund, U., Hanes, J.A., Gladkochub, D.P., Okrugin, A.V., Kolotilina, T., Mekhonoshin, A.S., Bleeker, W., LeCheminant, A.N., Buchan, K.L., Chamberlain, K.R., Didenko, A.N., 2016. Long-lived connection between southern Siberia and northern Laurentia in the Proterozoic. Nature Geosci. (in press).

Evins, L.Z., Jourdan, F., Phillips, D., 2009. The Cambrian Kalkarindji Large Igneous Province: Extent and characteristics based on new $^{40}Ar/^{39}Ar$ and geochemical data. Lithos 110, 294–304. doi:10.1016/j.lithos.2009.01.014.

Feybesse, J.L., Johan, V., Triboulet, C., Guerrot, C., Mayaga-Mikolo, F., Bouchot, V., Eko N'dong, J., 1998. The West Central African belt: a model of 2.5–2.0 Ga accretion and two-phase orogenic evolution. Precambrian Res. 87, 161–216.

Figueiredo, F.T., De Almeida, R.P., Tohver, E., Babinski, M., Liu, D.-Y., Fanning, C.M., 2009. Neoproterozoic glacial dynamics revealed by provenance of diamictites of the Bebedouro Formation, São Francisco Craton, Central Eastern Brazil. Terra Nova 21, 375–385.

Gerstenberger, H. Haase, G., 1997. A highly effective emitter substance for mass spectrometric Pb isotope ratio determinations. Chem. Geol. 136, 309–312.

Gladkochub, D.P., Pisarevsky, S.A., Donskaya, T.V, Ernst, R.E., Wingate, M.T., Söderlund, U., Mazukabzov, A.M., Sklyarov, E.V., Hamilton, M.A., Hanes, J.A., 2010a. Proterozoic mafic magmatism in Siberian craton: an overview and implications for paleocontinental reconstruction. Precambrian Res. 183, 660–668.

Gladkochub, D.P., Pisarevsky, S.A., Ernst, R., Donskaya, T.V., Soderlund, U., Mazukabzov, A.M., Hanes, J., 2010b. Large Igneous Province of about 1750 Ma in the Siberian Craton. Dokl. Earth Sci. 430 (2), 168–171.

Guimarães, J.T., Teixeira, L.R., Silva, M.G., Martins, A.A.M., Filho, E.L.A., Loureiro, H.S.C., Arcanjo, J.B., Dalton de Souza, J., Neves, J.P., Mascarenhas, J.F., Melo, R.C., Bento, R.V., 2005. Dataçxes U–Pb em rochas magmáticas intrusivas no Complexo Paramirim e no Rifte Espinhaço: uma contribuição ao estudo da evolução geocronológica da Chapada Diamantina. III Simpósio sobre o Cráton do São Francisco (Symposium on the São Francisco Craton), Salvador, pp. 159–161.

Hamilton, M.A., Buchan, K.L., 2010. U–Pb geochronology of the Western Channel diabase, northwestern Laurentia: implications for a large 1.59 Ga magmatic province, Laurentia's APWP and paleocontinental reconstructions of Laurentia, Baltica and Gawler craton of southern Australia. Precambrian Res. 183, 463–473.

Irvine, T.N., Baragar, W.R.A., 1971. A guide to the chemical classification of the common volcanic rocks. Can. J. Earth Sci. 8, 523–548.

ISC (Interdepartmental Stratigraphic Committee) of Russia, 2006. Stratigraphic Code of Russia [in Russian], third ed. VSEGEI Press, St. Petersburg.

Ivanov, A.V., He, H.-Y., Yan, L.-K., Ryabov, V.V., Shevko, A.Y., Palesskii, S.V., Nikolaeva, I.V., 2013. Siberian Traps large igneous province: evidence for two flood basalt pulses around the Permo-Triassic boundary and in the Middle Triassic, and contemporaneous granitic magmatism. Earth Sci. Rev. 122, 58–76.

Jaffey, A.H., Flynn, K.F., Glendenin, L.E., Bentley, W.C., Essling, A.M., 1971. Precision measurement of half-lives and specific activities of ^{235}U and ^{238}U. Phys. Rev. 4, 1889–1906.

Kamo, S.L. Czamanske, G.K., Amelin, Y., Fedorenko, V.A., Davis, D.W., Trofimov, V.R., 2003. Rapid eruption of Siberian flood-volcanic rocks and evidence for coincidence with the Permian–Triassic boundary and mass extinction at 251 Ma. Earth Planet. Sci. Lett. 214, 75–91.

Krogh, T.E., 1973. A low contamination method for hydrothermal decomposition of zircon and extraction of U and Pb for isotopic age determinations. Geochim. Cosmochim. Acta 37, 485–494.

Kuskov, O.L., Kronrod, V.A., Prokof'ev, A.A., 2011. Thermal structure and thickness of the lithospheric mantle underlying the Siberian Craton from the "Kraton" and "Kimberlit" superlong seismic profiles. Izvestiya, Physics of the Solid Earth 47 (3), 155–175.

Kuteynikov, E.S., Orlov, I.M., Tolchel'nikov, Yu.N., 1967. Late Proterozoic traps of the Anabar anteclise. Geologiya i Geofizika 8 (2), 121–123.

Lightfoot, P.C., Naldrett, A.J., Gorbachev, N.S., Fedorenko, V.A., Hawkesworth, C.J., Hergt. J., Doherty, W., 1994. Chemostratigraphy of Siberian Trap lavas, Noril'sk District, Russia: implications for the source of flood basalt magmas and their associated Ni–Cu mineralization, in: Lightfoot, P.C., Naldrett, A.J. (Eds.), Proc. Sudbury–Noril'sk Symposium. Ontario Geological Survey, Toronto, Vol. 5, pp. 283–312.

Ludwig, K.R., 2003. Isoplot 3.70. A geochronological toolkit for Microsoft Excel, Vol. 4. Berkeley Geochronology Center Special Publication.

Naldrett, A.J., 2010. Secular variation of magmatic sulfide deposits and their source magmas. Econ. Geol. 105, 669–688.

Neumann, E.-R., Svensen, H., Galerne, C.Y., Planke, S., 2011. Multistage evolution of dolerites in the Karoo Large Igneous Province, Central South Africa. J. Petrol. 52, 959–984.

Nilsson, M.K.M., Klausen, M.B., Söderlund, U., Ernst, R.E., 2013. Precise U–Pb ages and geochemistry of Paleoproterozoic mafic dikes from southern West Greenland: Linking the North Atlantic and the Dharwar Cratons. Lithos 174, 255–270.

Okrugin, A.V., Oleinikov, B.V., Savvinov, V.T., Tomshin, M.D., 1990. Late Precambrian dike swarms of the Anabar Massif, Siberian Platform, USSR, in: Parker, A.J., Rickwood, P.C., Tucker, D.H. (Eds.), Mafic Dikes and Emplacement Mechanisms. Balkema, Rotterdam, pp. 529–533.

Pearce, J.A., 1996. A user's guide to basalt discrimination diagrams, in: Wyman, D.A. (Ed.), Trace Element Geochemistry of Volcanic Rocks: Applications for Massive Sulphide Exploration. Geol. Assoc. Can. Short Course Notes 12, 79–113.

Pearce, J.A., 2008. Geochemical fingerprinting of oceanic basalts with applications to ophiolite classification and the search for Archean oceanic crust. Lithos 100, 14–48.

Pearce, J.A., Cann, J.R., 1973. Tectonic setting of basic volcanic rocks determined using trace element analyses. Earth Planet. Sci. Lett. 19, 290–300.

Puchkov, V.N., Bogdanova, S.V., Ernst, R.E., Kozlov, V.I., Krasnobaev, A.A., Söderlund, U., Wingate, M.T.D., Postnikov, A., Sergeeva, N.D., 2013. The ca. 1380 Ma Mashak igneous event of the Southern Urals. Lithos 174, 109–124.

Reichow, M.K., Pringle, M.S., Al'Mukhamedov, A.I., Allen, M.B., Andreichev, V.L., Buslov, M.M., Davies, C.E., Fedoseev, G.S., Fitton, G., Inger, S., Medvedev, A.Y., Mitchell, C., Puchkov, V.N., Safonova, I.Y., Scott, R.A., Saunders, A.D., 2009. The timing and extent of the eruption of the Siberian Traps large igneous province: implications for the end-Permian environmental crisis. Earth Planet. Sci. Lett. 277 (1–2), 9–20.

Rosen, O.M., Manakov, A.V., Serenko, V.P., 2005. Paleoproterozoic collisional system and diamondiferous lithospheric keel of the Yakutian kimberlite province. Russian Geology and Geophysics (Geologiya i Geofizika) 46 (12), 1237–1251 (1259–1272).

Ryabov, V.V., Shevko, A.Ya., Gora, M.P., 2014. Trap Magmatism and Ore Formation in the Siberian Noril'sk Region, Vol. 1: Trap Petrology. Springer [Translated from Russian: Ryabov, V.V., Shevko, A.Ya., Gora, M.P., 2000. Magmatic Formations of the Norilsk Region, Vol. 1: Trap Petrology. Nonparel, Novosibirsk].

Sandeman, H.A., Ootes, L., Cousens, B., Killian, T., 2014. Petrogenesis of Gunbarrel magmatic rocks: homogeneous continental tholeiites associated with extension and rifting of Neoproterozoic Laurentia. Precambrian Res. 252, 166–179.

Schmitt, A.K., Chamberlain, K.R., Swapp, S.M., Harrison, T.M., 2010. In situ U–Pb dating of micro-baddeleyite by secondary ion mass spectrometry. Chem. Geol. 269 (3–4), 386–395. doi:10.1016/j.chemgeo.2009.10.013.

Shervais, J. W., 1982. Ti-V plots and the petrogenesis of modern and ophiolitic lavas: Earth Planet. Sci. Lett. 59 (1), 101–118.

Silveira, E.M., Söderlund, U., Oliveira, E.P., Ernst, R., Menezes Leal, A.B., 2013. First precise U–Pb baddeleyite ages of 1500 Ma mafic dikes from the São Francisco Craton, Brazil, and tectonic implications. Lithos 174, 144–156.

Söderlund, U., Johansson, L., 2002. A simple way to extract baddeleyite (ZrO_2). Geochem. Geophys. Geosyst. 3 (2), doi: 10.1029/2001GC000212.

Veselovskiy R., Pavlov V., 2009. New paleomagnetic pole from Precambrian magmatic bodies of the Kotuy river basin (northwestern part of the Siberian platform). Geophysical Research Abstracts, Vol. 11, EGU2009-10598. EGU General Assembly 2009.

Veselovskiy, R.V., Petrov, P.Yu., Karpenko, S.F., Kostitsyn, Yu.A., Pavlov, V.E., 2006. New paleomagnetic and isotopic data on the Mesoproterozoic igneous complex on the northern slope of the Anabar uplift. Dokl. Earth Sci. 411 (8), 1190–1194.

Winchester, J.A., Floyd, P.A., 1977. Geochemical discrimination of different magma series and their differentiation products using immobile elements. Chem. Geol. 20, 325–343.

Wingate, M.T.D., Compston, W., 2000. Crystal orientation effects during ion microprobe U–Pb analysis of baddeleyite. Chem. Geol. 168, 75–97.

Wingate, M.T.D., Pisarevsky, S.A., Gladkochub, D.P., Donskaya, T.V., Konstantinov, K.M., Mazukabzov, A.M., Stanevich, A.M., 2009. Geochronology and paleomagnetism of mafic igneous rocks in the Olenek Uplift, northern Siberia: implications for Mesoproterozoic supercontinents and paleogeography. Precambrian Res. 170, 256–266.